Nephron progenitors rhythmically alternate between renewal and differentiation phases that synchronize with kidney branching morphogenesis

Sachin N. Davis[1,2]*, Samuel H. Grindel[1,2]*, John M. Viola[1,2], Grace Y. Liu[1,2], Jiageng Liu[1,2], Grace Qian[1,2], Catherine M. Porter[1,2], Alex J. Hughes[1-6]

[1]Department of Bioengineering, University of Pennsylvania, Philadelphia, 19104, PA, USA.
[2]Bioengineering Graduate Group, University of Pennsylvania, Philadelphia, 19104, PA, USA.
[3]Cell and Molecular Biology Graduate Group, University of Pennsylvania, Philadelphia, 19104, PA, USA.
[4]Department of Cell and Developmental Biology, University of Pennsylvania, Philadelphia, 19104, PA, USA.
[5]Center for Soft and Living Matter, University of Pennsylvania, Philadelphia, 19104, PA, USA.
[6]Institute for Regenerative Medicine, University of Pennsylvania, Philadelphia, 19104, PA, USA.

*These authors contributed equally

Abstract

The mammalian kidney achieves massive parallelization of function by exponentially duplicating nephron-forming niches during development. Each niche caps a tip of the ureteric bud epithelium (the future urinary collecting duct tree) as it undergoes branching morphogenesis, while nephron progenitors within niches balance self-renewal and differentiation to early nephron cells. Nephron formation rate approximately matches branching rate over a large fraction of mouse gestation, yet the nature of this apparent pace-maker is unknown. Here we correlate spatial transcriptomics data with branching 'life-cycle' to discover rhythmically alternating signatures of nephron progenitor differentiation and renewal across Wnt, Hippo-Yap, retinoic acid (RA), and other pathways. We then find in human stem-cell derived nephron progenitor organoids that Wnt/β-catenin-induced differentiation is converted to a renewal signal when it temporally overlaps with YAP activation. Similar experiments using RA activation indicate a role in setting nephron progenitor exit from the naive state, the spatial extent of differentiation, and nephron segment bias. Together the data suggest that nephron progenitor interpretation of consistent Wnt/β-catenin differentiation signaling in the niche may be modified by rhythmic activity in ancillary pathways to set the pace of nephron formation. This would synchronize nephron formation with ureteric bud branching, which creates new sites for nephron condensation. Our data bring temporal resolution to the renewal vs. differentiation balance in the nephrogenic niche and inform new strategies to achieve self-sustaining nephron formation in synthetic human kidney tissues.

Introduction

Collectives of nephron progenitor cells cap the branching ureteric bud tree during kidney development, periodically contributing cells that condense into discrete pre-tubular aggregates (PTAs) — the earliest nephron stage. This process occurs continuously but asynchronously across ureteric bud tips[1]. Understanding the rate at which nephrons form is an important factor in addressing person-to-person variability in nephron endowment, which impacts adult kidney function[2–6]. A better understanding would also inform *in vitro* synthetic kidney tissue production using organoids, where contemporary protocols produce nephrons in a single inductive wave rather than in sustained waves[7,8]. *In vivo*, nephron progenitor ('cap mesenchyme') niches balance renewal vs. differentiation by interpreting autonomous cues and those from adjacent ureteric bud and stromal cell populations[9] (**Fig. 1A,B**). Only a portion of a cap's progenitors commit to each successive nephron, enabling niches to maintain persistent progenitor pools during development[1]. It is known that FGF/EGF/MAPK[10–13], PI3K/Akt[14], Wnt/β-catenin (low/high)[15–18], Hippo[19,20], JAK/STAT[21,22], TGFβ/BMP[23,24], and Notch[25–27] pathways are important for progenitor renewal and differentiation. However, the relative rates of renewal vs differentiation may not be constant in time, since cells commit as transient avalanche-like streams from the cap mesenchyme into discrete PTAs[28]. Indeed, we recently reported that nephron formation rate is not constant over the ureteric bud branching cycle, but rather nephron formation pauses after each branch event and resumes before the next one[29]. These observations suggest both a switch-like response of progenitors to inductive cues as single cells and an avalanche-like response to inductive cues as cell collectives. The Wnt ligand Wnt9b presented to the cap by the nearby ureteric bud is thought to be a dominant

cue[15,18,30]. The switch-like response may be explained by a transition in SIX2/TCF/LEF/β-catenin factor occupancy at target genes upon rising β-catenin levels caused by stochastic exposure of cells to Wnt9b as they migrate in and out of several sub-domains in the niche[16,17,23,28,31–34]. However, the origin of avalanche-like commitment of batches of cells to early nephron aggregates is unknown. This may relate to feedback associated with the ureteric bud branching 'life-cycle'[17] (**Fig. 1C,D**), potentially through the effect of its curvature on Wnt9b concentration gradients[35], although this is debated[30]. Indeed, any life-cycle-dependent change in nephron progenitor contact area with the ureteric bud or stroma[20], 'mixing' state among these compartments[36–38], or niche mechanical microenvironment[29] are reasonable hypotheses yet to be disproven.

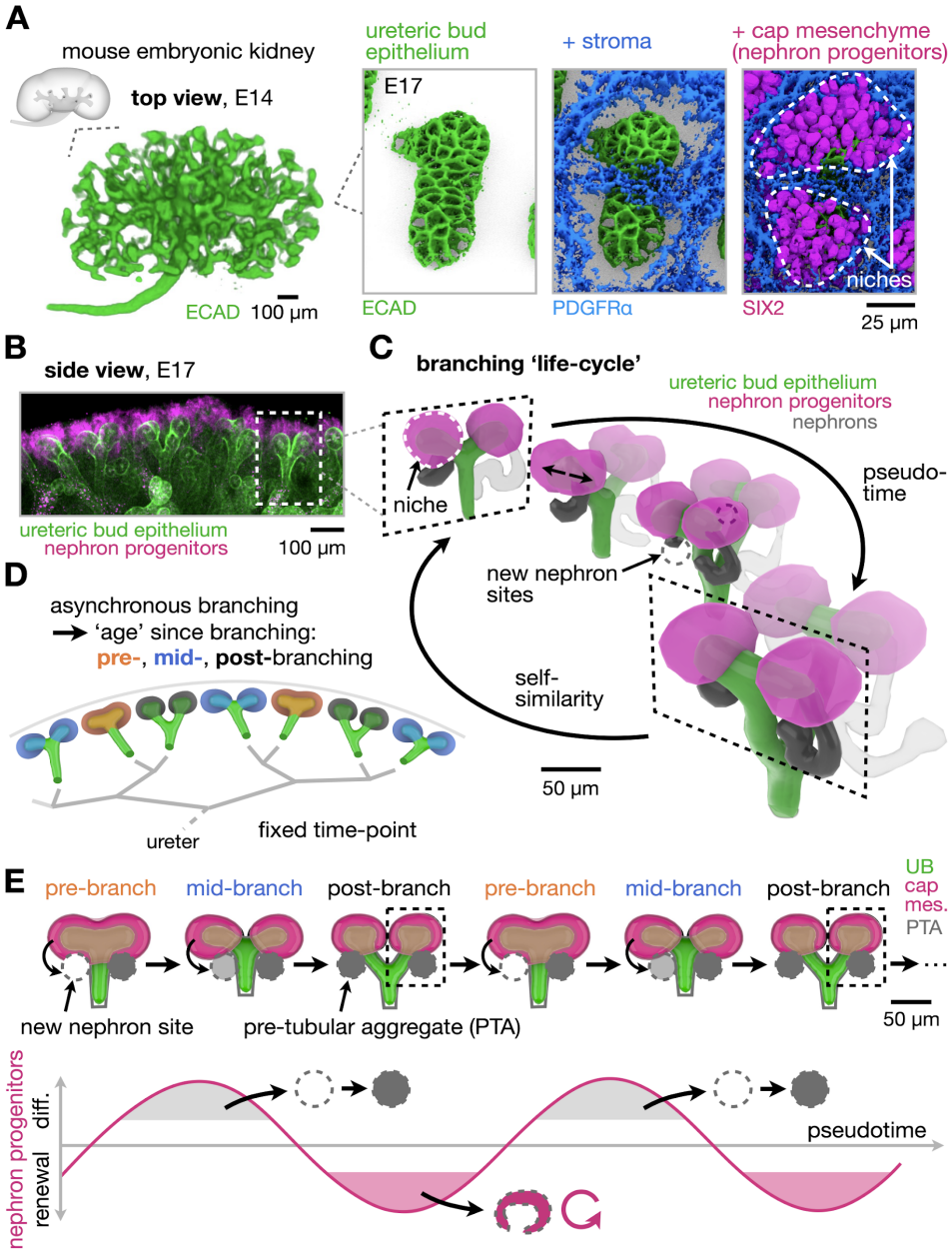

Fig. 1: Defining branching 'life-cycle'-dependent regulation in nephron progenitor niches. (**A**) Confocal immunofluorescence renderings of the mouse embryonic kidney ureteric bud tubule tree at embryonic day 14 (E14) and example niches at its tips at E17. Each tip is surrounded by SIX2+ nephron progenitors (the cap mesenchyme) and bordered by PDGFRA+ stroma. (**B**) Side view of several niches at E17 by confocal immunofluorescence. (**C**) Schematic of ureteric bud branching, which causes niches traveling with them to divide periodically. Branching can be described as a 'life-cycle' due to self-similarity between a branch just beginning to divide and one of the daughters formed after branching. Since branching occurs asynchronously among ureteric bud tips/niches, a 'pseudo-time' concept enables their life-cycles to be aligned with each other. (**D**) At a given real time-point, niches of different age in branching pseudotime co-exist. (**E**) Schematic hypothesis for 'just in time' contribution of committing nephron progenitors to condensation sites newly formed by branching morphogenesis. Nephron progenitors would renew between branching events (cap mes.: cap mesenchyme).

Here we find that the avalanche-like commitment of nephron progenitors coincides with rhythmic transcriptional changes across several pathways synchronized with the ureteric bud branching life-cycle, interspersed with pauses[29] in which nephron progenitors renew. This may act to match nephron formation rate to the ureteric bud branching rate. We next transfer this emerging control principle to a human induced pluripotent stem cell (iPSC)-derived nephron progenitor organoid system. Overlapping or staggered activation of the candidate rhythmic pathways YAP or retinoic acid successfully shifts interpretation of an inductive Wnt/β-catenin signaling cue by nephron progenitors to affect renewal vs. differentiation balance and nephron size/segment balance. These data establish a rhythmic homeostatic principle of nephrogenic niche regulation that achieves 'just in time' delivery of committing cells to nephron condensation sites newly formed by branching (**Fig. 1E**). This principle presents the opportunity to create self-sustaining nephrogenic niches *in vitro* by mimicking cycles of alternating differentiation and renewal cues.

Results

Pseudo-time ordering of niche transcriptomes to enrich for correlations between nephron progenitor state and ureteric bud branching life-cycle

The rates of nephron formation and ureteric bud branching in the mouse embryonic kidney are equivalent from E15-E22[1], suggesting that a type of pace-maker synchronizes the two processes. We wondered if this pace-maker would manifest in a cyclical transcriptional state of nephron progenitors over the branching life-cycle. This required us to 1) sequence nephron progenitors from many separate niches, and 2) assign niches to 'pre-branching', 'mid-branching', and 'post-branching' 'age' groups before comparing gene expression between them. To do so we turned to Nanostring GeoMx spatial sequencing technology[39], which performs multiplexed bulk RNA sequencing within manually annotated regions of interest (ROIs). GeoMx is performed on 5 µm-thick tissue sections. Since the kidney surface is curved, we partially flattened embryonic day 17 (E17) mouse kidneys prior to sectioning in order to sequence ROIs at the same *z*-depth from the organ surface (**Fig. 2A**, **Methods**). We drew ROIs around SIX2+ nephron progenitor clusters associated with 47 niches and sequenced each niche separately. We next classified the age of the niches associated with each ROI relative to the ureteric bud branching cycle using two qualitative metrics (branch point position and cap mesenchyme connectivity, **Fig. 2B,C**). As expected, median gene expression scaled with ROI area, which normalization compensated for (**Fig. 2D**, **Methods**). The cap mesenchyme ROIs were drawn to exclude stromal cells, nephron connecting segments, and PNA lectin-stained ureteric bud cells that are each readily distinguished from nephron progenitors by their morphology and location in the niche. Other committed cells in pre-tubular aggregates, renal vesicles, and later stages were intrinsically excluded during sample preparation because they are found in deeper sectioning planes. While these off-target tissue compartments were not sampled in the same experiment, expression of canonical markers for them were not significantly differentially expressed between ROIs associated with pre-, mid-, and post-branching ureteric bud tips (**Fig. 2E**). These data reflect successful recovery of transcriptomes from nephron progenitor collectives associated with individual niches using GeoMx and suggest that any contamination by off-target cells was consistent among ROIs across the age groups.

Nephron progenitor niche transcriptomes reveal rhythmic changes in renewal and differentiation pathways over the ureteric bud branching life cycle

Starting from our GeoMx results, we sought to detect transcriptional differences between nephron progenitor collectives in pre-, mid-, and post-branching niches. Non-linear dimensional reduction by tSNE largely grouped ROIs by their age categories, showing some global transcriptional distinction between them (**Fig. 3A**). We next moved to ('all-gene') differential expression analysis and validated expression of certain transcripts in the cap mesenchyme by RNA fluorescence in-situ hybridization (HCR RNA-FISH)[40–42], indicated with a dagger (†) throughout the text (**Fig. S1**). *Retsat*, *Mucl1*, and *Mrps17*† were hits at false discovery rate (FDR) < 0.1, and *Stox2* at FDR < 0.3 (**Fig. 3B**). Significance testing here was robust to randomizing the age categories of the ROIs (**Fig. S2**). These hits together suggest possible differential regulation of retinoic acid (*Retsat*), Wnt/β-catenin (*Mucl1*)[43], TGFβ (*Stox2*)[44], and PI3K/Akt (*Mrps17*)[45] signaling pathways in nephron progenitors over the branching life-cycle (**Note S1**).

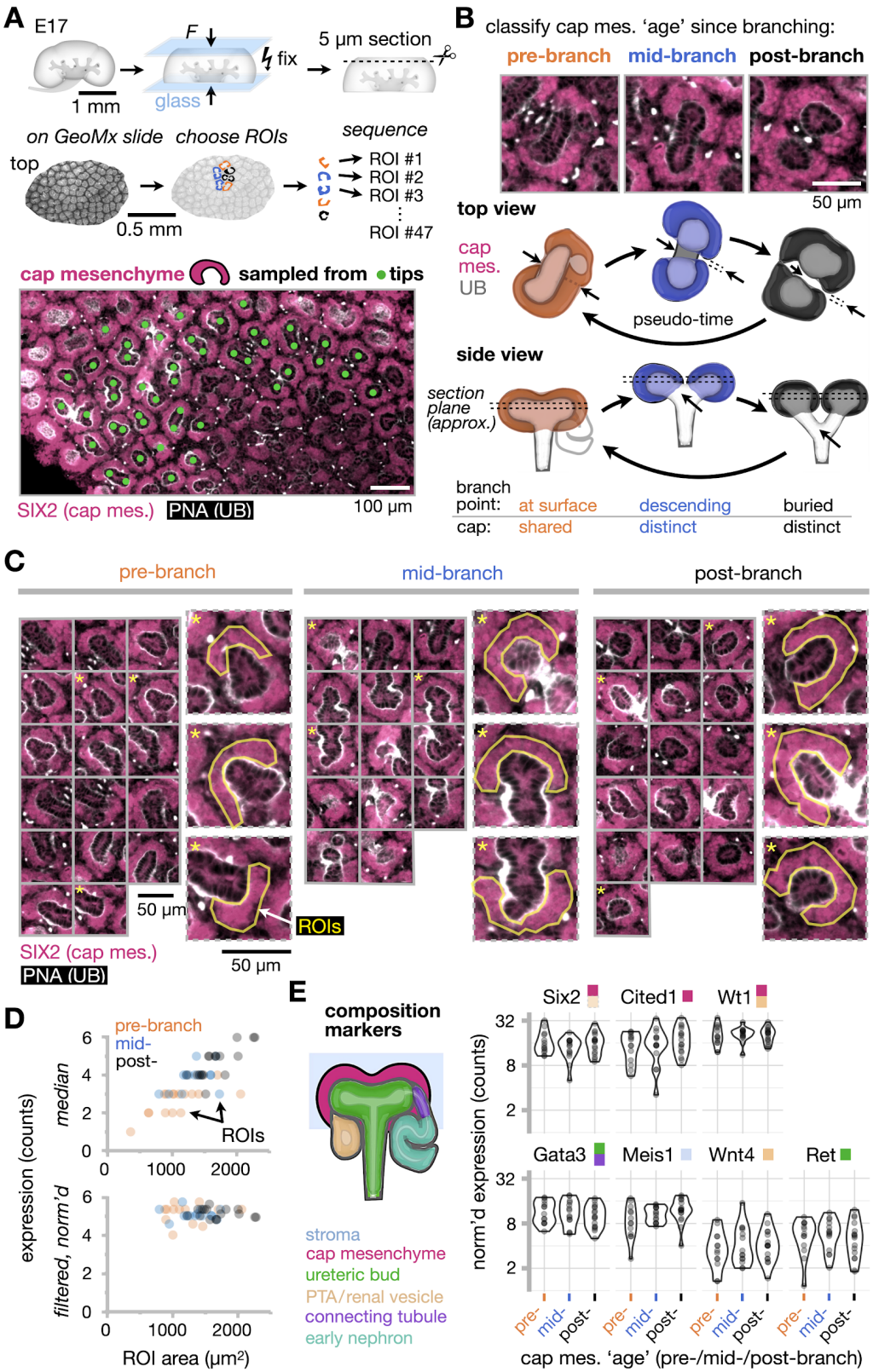

Fig. 2: Collecting and classifying bulk transcriptomes of nephron progenitor niches from three branching life-cycle stages. (**A**) *Top*, Schematic of E17 kidney flattening, sectioning and processing for GeoMx spatial sequencing. Transcripts from cap mesenchyme cells in 47 individual regions of interest (ROIs) were collected and sequenced. *Bottom*, fluorescence micrograph of the slice used in this study. Ureteric bud tips from which cap mesenchyme transcriptomes were sampled are annotated. (**B**) *Top*, three example cap mesenchyme niches scored for life-cycle stage. *Middle*, cartoons representing niche morphology in top and side views. *Bottom*, Qualitative life-cycle metrics (branch point appearance in *z* and cap mesenchyme connectivity) used to score each ROI as pre-, mid-, or post-branching. (**C**) Fluorescence micrographs of all niches after scoring. *Insets*, example niches and GeoMx ROIs. (**D**) Plots of median gene expression vs. GeoMx ROI area before and after Q3 normalization, showing correction for systematic variation in ROI area between pre-, mid-, and post-branching niches. Points represent individual ROIs (cap mesenchyme niches). (**E**) Normalized expression of marker genes for cap mesenchyme and surrounding tissue compartments in GeoMx ROIs (PTA: pre-tubular aggregate; cap mes.: cap mesenchyme). Colored squares indicate tissue compartments associated with each marker.

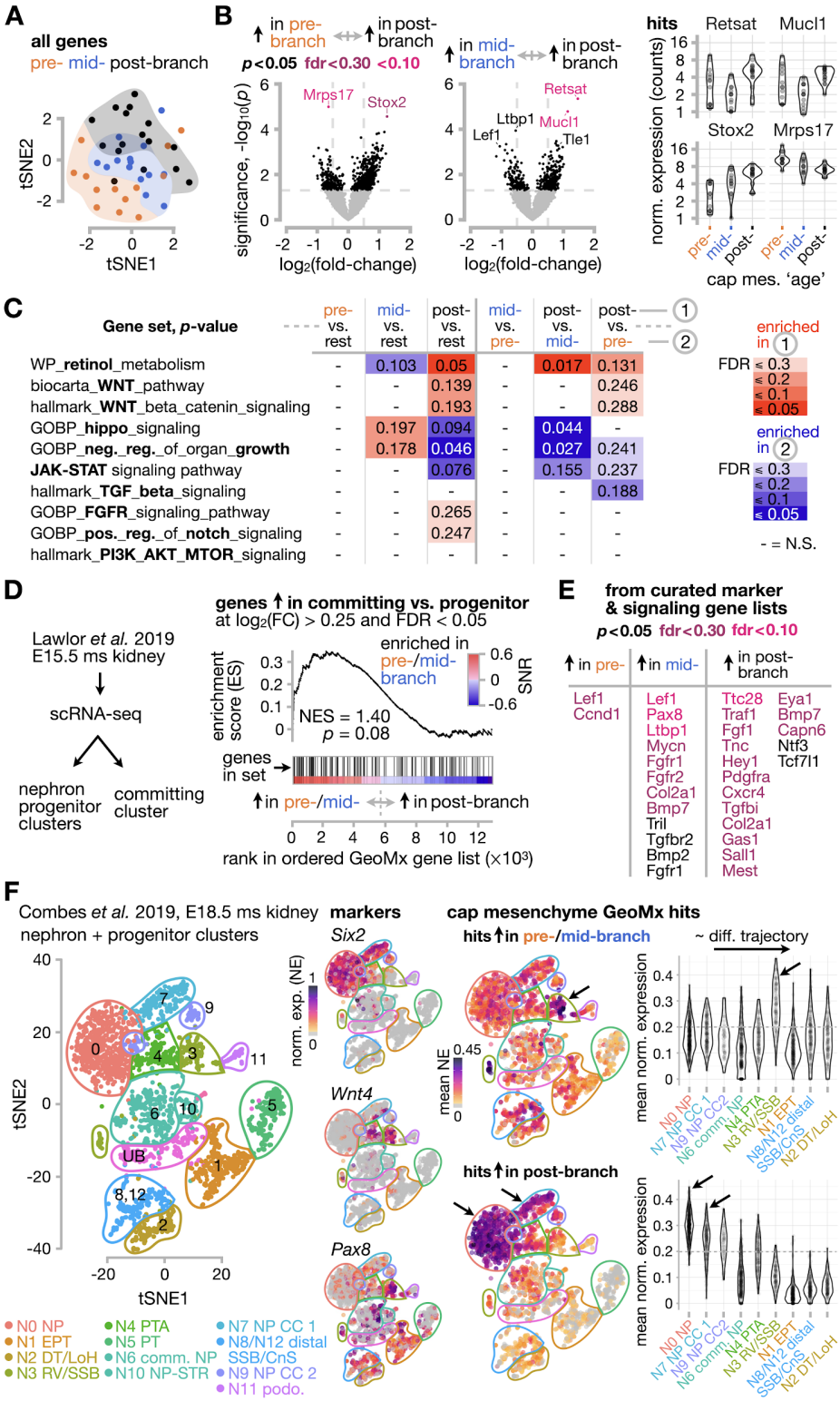

Fig. 3: The cap mesenchyme transcriptome at E17 varies in several renewal and differentiation pathways depending on ureteric bud branching life-cycle stage. (**A**) tSNE plot shaded by niche 'age' since branching. Envelopes are a visual aid, bounding >75% of the ROIs in each category. (**B**) All-gene differential expression analysis and violin plots for hits significant at false discovery rate (FDR) < 0.3. (**C**) Summary table of false-discovery rates (FDRs) for curated gene set enrichment analysis (GSEA). Gene set details and analyses are provided in **Fig. S3**. (**D**) GSEA results for a gene set created from those differentially expressed in 'committing' nephron progenitors vs. nephron progenitors based on data from Lawlor *et al.* 2019. (**E**) Summary table for differential expression of curated marker and signaling genes relevant to nephron progenitor renewal and early differentiation. (**F**) tSNE plots of E18.5 mouse kidney scRNA-seq data from Combes *et al.* 2019 showing: *left*, Cell type annotations (NP: nephron progenitor, EPT: early proximal tubule, DT/LoH: distal tubule/loop of Henle, RV/SSB: renal vesicle/S-shaped body, PTA: pretubular aggregate, PT: proximal tubule, comm.: committing, NP-STR: stromal-like NP, CC: cell cycle-associated, CnS: connecting segment, podo.: podocyte), *middle*, feature plots of nephron progenitor (*Six2*) and differentiation (*Wnt4, Pax8*) markers. *Right*, feature and violin plots by cell type of mean normalized expression of rhythmic GeoMx hits from (E) in Combes scRNA-seq clusters.

We moved to gene-set enrichment analysis (GSEA)[46] to examine these pathways and others with known roles in nephron progenitor renewal, priming, and differentiation at higher sensitivity (**Fig. 3C, Fig. S3**, **Note S2**, **Introduction**). We found that gene sets describing 1) retinol metabolism, 2) Wnt pathway, 3) Wnt targets and, with weaker significance, 4) FGFR signaling and 5) positive regulation of Notch signaling genes were enriched in nephron progenitors from post-branching vs. pre-/mid-branching niches (minimum FDRs = 0.017, 0.14, 0.19, 0.27, and 0.25 respectively). Closer inspection of enriched transcripts suggested that Wnt/β-catenin and retinoic acid signaling may actually be higher in nephron progenitors in pre-/mid-branching niches (**Note S3**). Gene sets describing 1) Hippo signaling (**Note S3**, and similarly,) 2) negative regulation of organ growth, 3) JAK-STAT signaling (notably *Hras*[10]), and 4) TGFβ signaling were enriched in nephron progenitors from pre-/mid-branching vs. post-branching niches (minimum FDRs = 0.044, 0.027, 0.076, and 0.188 respectively). These data are evidence that the transcriptional state of cap mesenchyme populations is not monolithic over the ureteric bud branching cycle; rather that nephron progenitors change periodically as a whole or through transitions between sub-populations in pathways relevant to renewal vs differentiation decision-making.

We sought additional evidence for this by testing if, on average, nephron progenitors change their 'priming state' as a function of the branching life-cycle. We re-analyzed scRNA-seq data in Lawlor *et al.* 2019[32] to retrieve a list of genes that are differentially expressed between 'committing' nephron progenitors vs. naive nephron progenitors in E15.5 mouse kidneys. This gene set was enriched in pre-/mid-branching vs. post-branching niches at $p = 0.08$ (**Fig. 3D, Fig. S4**). These data support a rhythmic change in the 'priming state' of nephron progenitors synchronized with the branching morphogenesis cycle.

With this evidence for rhythmic regulation of GSEA and progenitor commitment gene sets, we sought to perform gene-by-gene differential expression analysis of a more diverse range of 1) cell identity, and 2) signaling markers relevant to nephron progenitor renewal/differentiation. We created two mutually exclusive lists from literature sources for this 'curated-gene' analysis[10,14,18,19,23,25,28,32,34,36,47–60] (**Table S1**), scraping genes from scRNA-seq data and triaging them if they lacked a supporting study in nephron development, lacked expression in nephron progenitors, lacked relevance to the correct early commitment stage, and/or were redundant with other marker(s) or isoforms. Differential expression analysis as a function of the branching life-cycle returned the Wnt9b/β-catenin target genes *Lef1*[18,25] and *Pax8*[18,61], the TGFβ signaling factor *Ltbp1*†[58,62], and the cell cycle factor *Ttc28*†[32,63] as hits at FDR < 0.1 (**Fig. 3E, Fig. S5**). The first two are of particular note since *Lef1* is one of the first markers of nephron induction, followed closely by *Pax8*[31,64]. A range of other genes relevant to or dependent on FGF, TGFβ, Hippo-YAP, and proliferation pathways emerged as branching life-cycle-dependent at FDR < 0.3 (**Note S4, Fig. 3E, Fig. S5**). This category also included *Pdgfra*, which we believe indicates rhythmic stromal cell intercalation into the cap mesenchyme niche during post-branching periods based on more detailed analysis (**Note S5, Fig. 3E, Fig. S5)**. These data complement the overall rhythmic priming signal, adding further specificity to branching life-cycle-correlated genes in several key nephrogenesis pathways, particularly downstream of Wnt.

Transcripts enriched in different branching life-cycle phases map to distinct progenitor/nephron sub-populations and exhibit rhythmic expression dynamics

We next sought to determine which cell states and types expressed rhythmic hits from the all-gene and curated-gene differential expression analyses. We first went back to the Lawlor *et al.* 2019 E15.5 scRNA-seq clusters. On average, hits associated with pre-/mid-branching niches were primarily found in committing nephron progenitors, while hits associated with post-branching niches were primarily found in uncommitted nephron progenitors and nephron progenitors having a stromal-like signature (**Note S5, Fig. S6**). We repeated this analysis for a higher-resolution E18.5 scRNA-seq dataset reported in Combes *et al.* 2019[47] (**Fig. 3F, Fig. S7**). We recovered similar nephron lineage clusters as Combes and again found a bias in expression of pre-/mid-branching hits vs. post-branching hits along the nephron progenitor differentiation trajectory, but this time without the stromal-like signature (**Note S5)**. Pre-/mid-branching hits (e.g. *Ccnd1*, *Lef1, Pax8, Ltbp1, Mycn, Fgfr2*) were enriched in renal vesicle and more mature clusters, while post-branching hits (e.g. *Ttc28*, *Traf1*, *Fgf1, Tnc, Tgfbi, Col2a1, Gas1, Mest, Eya1, Capn6*) were enriched in uncommitted and cell cycle-associated nephron progenitor clusters. These data suggest that all or a fraction of nephron progenitors shift from a differentiating to renewing character between pre-/mid- and post-branching phases.

To create a more continuous picture of transcript dynamics, we used unsupervised clustering using hits across the all-gene and curated-gene sets having FDR < 0.3 and $-\log_{10}(p) > 2$ (**Fig. 4A**). This roughly clustered nephron progenitor collectives from pre-, mid-, and post-branching niches. The clustering heatmap ordered genes in a wave-like fashion according to their up- and down-regulation along the pseudotime axis from pre- to mid- to post-branching niches. For example, *Lef1* and *Pax8* clustered together, both being upregulated around the transition from pre- to mid-branching and downregulated in post-branching niches. Several transcripts associated with FGF and TGFβ signaling peaked in mid-/post-branching (*Gas1*[17,65,66], *Fgf1*[10,47,48], *Fgfr1*[47,48,67], *Stox2*[44], *Tgfbi*[47,51,68]), and the YAP-dependent gene *Traf1*[19] along with *Ttc28*, *Retsat*, and *Mucl1* peaked in post-branching niches, continuing into pre-branching ones (formed as post-branching niches enter another round of branching), **Fig. 4A**, **Fig. S5**. The clustering data reinforce the notion of rhythmic, temporally staggered (out-of-phase) transcriptional regulation in several pathways associated with nephron progenitor maintenance and commitment over the branching life-cycle. The temporal relationship between WNT and FGF signaling pathway members/targets along with the GSEA and curated-gene analyses (**Fig. 3C-F**, **Fig. 4A**, **Fig. S3-6**) suggest that nephron progenitor niches may transition through alternating phases of differentiation (in early-middle stages of branching) and renewal (after branching has completed and as the next branching cycle approaches).

Protein-level validation confirms rhythmic priming, differentiation, and renewal signatures

We sought to validate a subset of the spatial sequencing hits using immunofluorescence in mouse embryonic kidneys, starting with hits primarily from the all-gene analysis. MUCL1, MRPS17, LTBP1, DHRS3, and CELSR1† antibodies yielded fluorescence consistent with non-specific background. RETSAT showed little protein-level expression in the cap mesenchyme, but did so in early distal nephron/connecting segment cells that are the first to be specified in early nephrons[28] (**Fig. S8**). RETSAT expression there could act to reduce retinoic acid signaling, potentially altering Wnt/β-catenin activation in the distal nephron[25,69,70], a point for future study.

We moved on to focus validation toward priming, differentiation, and renewal markers. Autocrine BMP7 primes nephron progenitors, sensitizing them to subsequent commitment induced by Wnt/β-catenin[23]. Prompted by a weak rhythmic signature for *Bmp7* (**Fig. 3E**, **Fig. S5**) and enrichment of the BMP7 target *Id1*[24] in pre-/mid-branching niches (**Figs. S3I, S4**), we stained for pSMAD1/5 signaling downstream of BMP7[23,24] (**Fig. 4B**). pSMAD1/5 was similarly enriched in pre-/mid-branching niches, indicating rhythmic priming of nephron progenitors early in the branching life-cycle.

We turned next to Wnt/β-catenin targets that mark nephron progenitor differentiation[17,18]. LEF1 staining peaked in nephron progenitors associated with mid-branching ureteric bud tips, similar to the GeoMx transcript-level data (**Fig. 4C**). The majority of the signal was contributed by rare LEF1+ ITGA8+ (low) cells typically at the edge of caps adjacent to the cleft between sister ureteric bud tips. These cells are presumably beginning to leave the niche while condensing into nearby pre-tubular aggregates (**Note S6**). Immunofluorescence for other Wnt9b targets[17,18] PAX8, ITGA8, and CCND1 also showed significant life-cycle correlation. PAX8 peaked in post-/pre-branching niches, lagging the mid-branching peak in *Pax8* transcript. This may reflect differences in post-transcriptional timescales (e.g. translation, degradation)[71] between LEF1 and PAX8. These data confirm rhythmic Wnt pathway activity at the protein level in nephron progenitors synchronized with the branching life-cycle, which is relevant to their differentiation[17], mesenchymal-to-epithelial transition[72], and later establishment of nephron polarity (proximal to distal)[25].

As an aside, *Pdgfra*† (a rhythmic hit in **Fig. 3E**) is curious since it is a stromal marker. The existence of a stromal-like nephron progenitor population is debated[47]. These cells appear to variable extents in published scRNA-seq datasets[32,47,66,73,74], however PDGFRA protein expression is rare in the mouse cap mesenchyme[47,73,75] (**Note S5, Fig. S6)**. PDGFRA staining validated life-cycle-correlated variation in the proportion of stromal-like nephron progenitors and/or stromal cell protrusion into the cap mesenchyme, likely the latter (**Fig. 4D**, **Note S5**). Whether stromal intercalation during the post-branching phase causes or results from nephron progenitor differentiation and segregation from the cap mesenchyme is a point for future study[38].

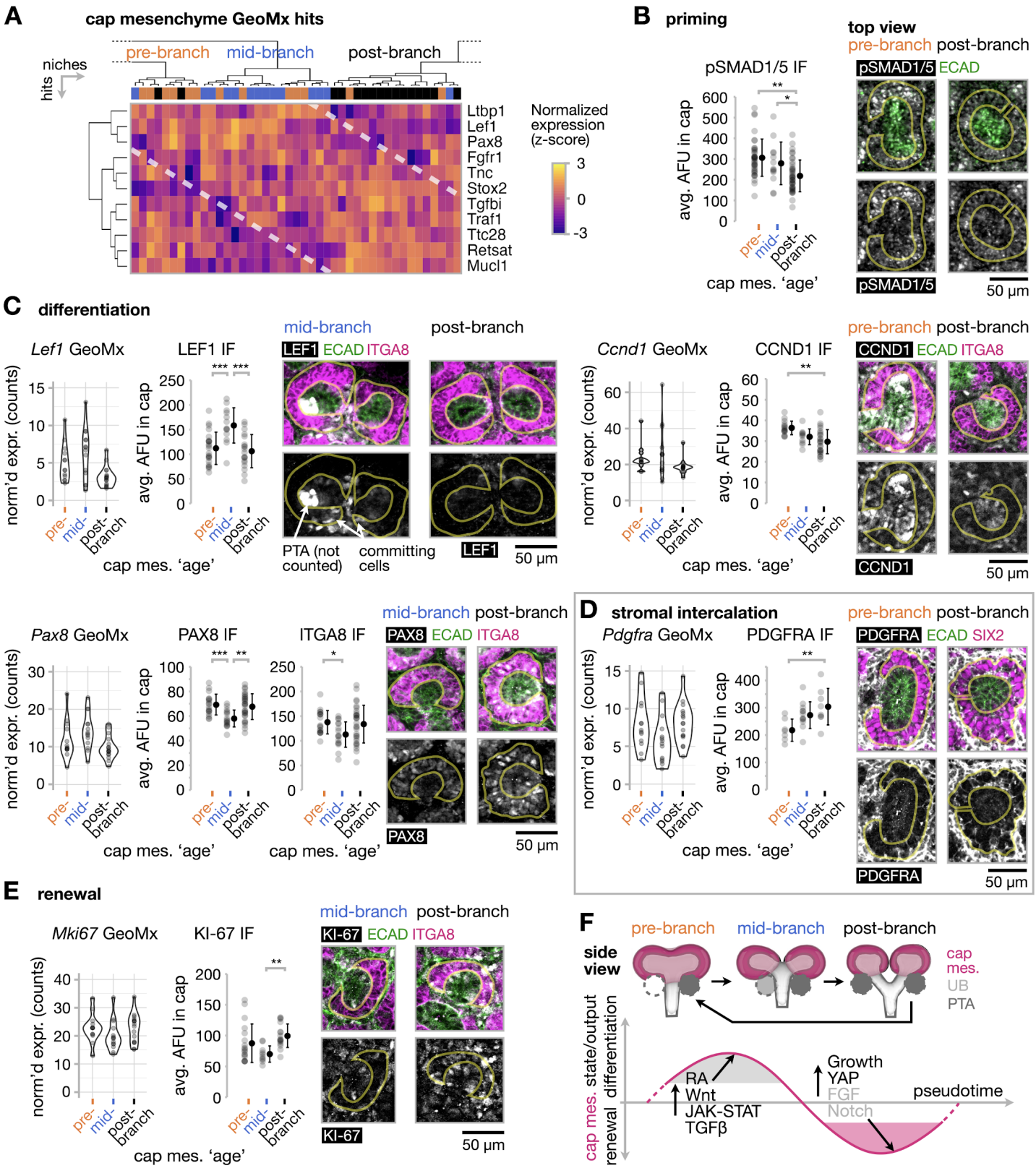

Fig. 4: Rhythmic priming/differentiation and renewal in the cap mesenchyme over the niche branching life-cycle. (**A**) Unsupervised clustering of differentially expressed curated genes reveals wave-like expression over pre-, mid-, and post-branching nephron progenitor niches (dotted lines added for emphasis). (**B-E**) Average arbitrary fluorescence (AFU) of hits in cap mesenchymes of pre-, mid-, and post-branching niches, with example confocal immunofluorescence images. Images at bottom show the isolated fluorescence channel for the marker of interest. (**F**) Schematic model depicting alternating differentiation (pre- and mid-branching) and renewal (post-branching) phases in the cap mesenchyme, annotated by associated GSEA signaling pathways/processes. For B-E each point represents one cap mesenchyme niche, $n > 12$ niches per category, mean ± S.D. One-way ANOVA, Tukey's test, *$p < 0.05$, **$p < 0.01$, ***$p < 0.001$.

Turning to cell renewal, our GSEA and curated-gene analyses suggested that nephron progenitors in post-branching niches may be more proliferative (**Fig. 3C,E,F**). The GeoMx data showed a decrease in the proliferation marker *Mki67* expression in mid-branching niches relative to a peak in post-branching ones (**Fig. 4E**). We stained for the corresponding protein KI-67, which marks cells in all active phases of the cell cycle, especially S-phase[76]. KI-67 correlated temporally with its transcript and was significantly increased in post-branching niches (**Fig. 4E**), reflecting an overall proliferation change or a change in the ratio of high/low proliferation sub-populations of nephron progenitors[1]. These data reinforce the notion that nephron progenitors favor renewal between branching events and differentiation during them (**Fig. 4F**).

Rhythmically regulated pathways in the mouse niche are sufficient to modify interpretation of Wnt differentiation signaling in human stem-cell derived nephron progenitors

Having validated rhythmic expression of several targets over the branching life-cycle in nephron progenitors, we sought to reconstitute rhythmic signaling in human iPSC-derived nephron progenitor organoid 'pucks' cultured at an air-liquid interface[77–79]. Despite some species-specific differences, these cells roughly transit through the same states when differentiated (transcriptionally and in protein marker expression) as nephron progenitors in the mouse niche[75,77,80–82]. A 'pulse' of Wnt/β-catenin activation via the GSK3β inhibitor CHIR 99021 is commonly used to increase differentiation efficiency of SIX2+ nephron progenitors in these protocols[77,80]. We reasoned that combining transient Wnt activation with simultaneous or staggered perturbation of candidate signaling pathways from our GeoMx screen would cause differences in nephron progenitor renewal vs. differentiation if rhythmic signaling was relevant to maintaining this balance. We focused on YAP and retinoic acid signaling due to the rhythmic Hippo signaling and retinol metabolism signatures we uncovered during gene set enrichment analysis (**Fig. 3C, Fig. S3A,E**), and due to their known roles in nephron progenitor decision-making. Increased YAP signaling *in vivo* and *in vitro* appears to drive nephron progenitor renewal at the expense of differentiation, and vice versa (despite some conflicting observations)[19,20,22,83–86]. According to our GeoMx analysis, Wnt/β-catenin activity is likely higher in nephron progenitors in pre-/mid-branching niches, while YAP activity is likely higher in post-branching niches (**Notes S3, S4**). Based on this we hypothesized that YAP contributes to nephron progenitor renewal in the post-branching phase. This motivated us to test both simultaneous and staggered Wnt and YAP activation for effects on cell renewal/differentiation via CHIR and the LATS kinase inhibitor (Yap activator) TRULI[87] in day 10 nephron progenitors derived from two separate iPSC lines (**Fig. 5A,B**). TRULI has recently been found to recruit YAP to the nucleus of iPSC-derived nephron progenitors and extend their long-term renewal in 2D culture, while retaining their nephron differentiation potential[84]. We verified that TRULI increases YAP nuclear recruitment and target gene expression (*CTGF*, *CYR61*) in our day 10 nephron progenitors by immunofluorescence and qPCR respectively (**Fig. S9**). We then found that TRULI increased the representation of SIX2+ nephron progenitors in organoids at day 12 only when it temporally overlapped the 2 hr CHIR pulse at day 10, but not when it chased the CHIR pulse for 2 hr (**Fig. 5C,D**). However, YAP activation suppressed differentiation of cells to the JAG1+ renal vesicle state at day 12 in either case (**Fig. 5D**), which also translated to lower nephron formation at day 25 (**Fig. 5E,F**). Changes in nephron composition among the conditions were minimal (**Fig. S10**). These data indicate that the basal YAP state in nephron progenitor organoids permits Wnt-induced differentiation, while YAP activation converts the same Wnt signal into a renewal signal when the two temporally overlap. This interaction may relate to the paradoxical requirement of Wnt/β-catenin for both nephron progenitor renewal and differentiation[88], namely that a rhythmic YAP signaling context could enable the niche to alternately favor each state given a consistent Wnt/β-catenin input *in vivo*.

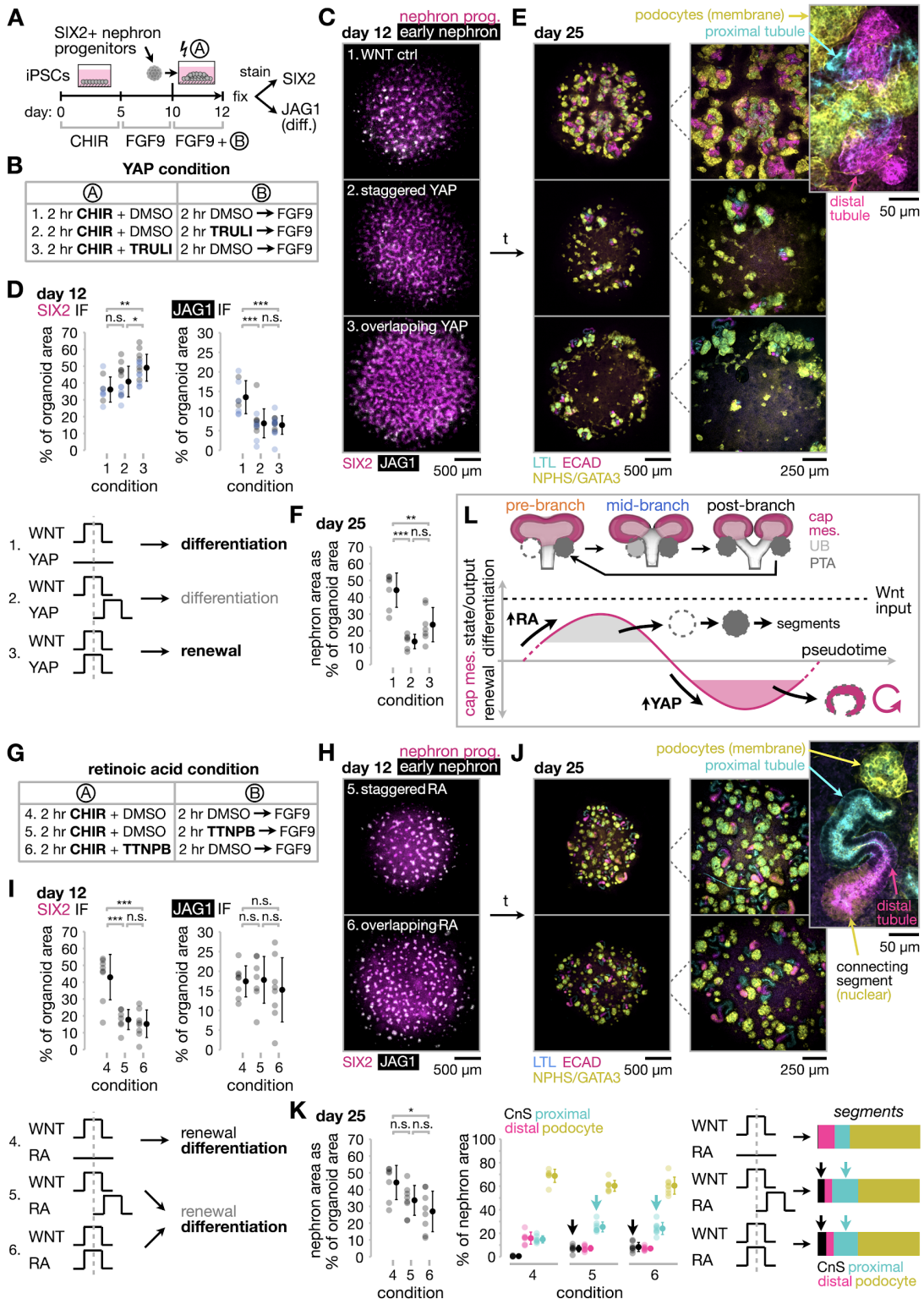

Fig. 5: YAP and RA status modify iPSC-derived nephron progenitor interpretation of Wnt/β-catenin differentiation signaling in 'puck' organoids. (**A**) Schematic workflow for nephron progenitor organoid differentiation and perturbation. (**B**) Table of perturbation conditions in the indicated phases of the differentiation schematic. Conditions 2 and 3 stagger or overlap the YAP agonist TRULI (4 µM) with standard 7 µM CHIR-induced differentiation in condition 1, respectively. (**C**) Confocal immunofluorescence images of representative SIX2^{EGFP} iPSC-derived organoids at the day 12 endpoint for nephron progenitor (SIX2) and early nephron (JAG1) markers. (**D**) *Top*, Plots of marker expression as % of organoid area for two replicates, one for 300,000 cells per puck at day 10 (black markers, MAFB^{BFP}:GATA3^{mCherry} iPSC line) and one for 150,000 cells per puck (blue markers, SIX2^{EGFP} iPSC line), $n > 2$ pucks per condition per replicate, mean ± S.D. *Bottom*, schematic of experiment outcomes. (**E**) Confocal immunofluorescence images of representative MAFB^{BFP}:GATA3^{mCherry} iPSC-derived organoids at the day 25 endpoint for nephron markers. (**F**) Plot of nephron cell area fraction relative to organoid area at day 25 for organoids in (E), $n > 5$ pucks per condition, mean ± S.D. (**G-J**) Similar data for MAFB^{BFP}:GATA3^{mCherry} iPSC-derived organoids perturbed with the retinoic acid analogue TTNPB, $n > 6$ pucks per condition, mean ± S.D. (**K**) *Left*, Plot of nephron cell area fraction relative to organoid area at day 25 for organoids in (J). *Right*, plot and schematic of nephron composition by cell type. Arrows indicate increase in connecting segment (CnS) and proximal tubule cells in conditions treated with TTNPB. $n > 6$ pucks per condition, mean ± S.D. Statistics in D,F,I,K are one-way ANOVA, Tukey's test, $^*p < 0.05$, $^{**}p < 0.01$, $^{***}p < 0.001$. (**L**) Schematic model for differential interpretation of Wnt input by nephron progenitors depending on branching life-cycle-associated rhythms in YAP and RA signaling.

While little is known about the role of retinoic acid after specification of nephron progenitors, microarray and qPCR analysis of RA-treated mouse embryonic kidney explants saw up-regulation in early nephron differentiation markers including *Lhx1* and *Wnt4* relative to untreated controls[89]. Retinoic acid synthesis enzymes are also expressed in early rat kidney connecting segments and renal vesicles[90]. Retinoic acid promotes proximal segment fate at the expense of distal segment in the zebrafish pronephros, but a similar role in the segmentation of mammalian nephrons has not yet been established[91,92]. According to our GeoMx analysis, retinoic acid signaling activity is likely higher in nephron progenitors in pre-/mid-branching niches, overlapping the peak of Wnt/β-catenin activity (**Note S3**). Based on this we hypothesized that RA contributes to nephron progenitor differentiation in the pre-/mid-branching phase. This motivated us to test both overlapping and staggered Wnt and retinoic acid activation for effects on cell renewal/differentiation via CHIR and the retinoic acid analogue TTNPB[93,94] in iPSC-derived nephron progenitors (**Fig. 5G**). We verified that TTNPB increases retinoic acid target gene expression (*RARB*, *CRABP2, CYP26A1*) in these cells by qPCR (**Fig. S9C**). Staggered or overlapping TTNPB exposure around the 2 hr CHIR pulse at day 10 reduced the SIX2+ cell fraction at day 12 and restricted SIX2 expression to spatially discrete colonies within organoids (**Fig. 5H,I**). Neither treatment timing affected the fraction differentiated to the JAG1+ state at day 12 (**Fig. 5I**), reflecting either off-target differentiation of SIX2+ cells or transit through to later differentiation states. Nephron formation by day 25 was robust for both TTNPB treatment timings (**Fig. 5J,K**). GATA3+ connecting segments appeared and nephrons were notably more spatially discrete, with frequent formation of polarized tubules with correct anatomical connectivity of connecting segment-distal tubule-proximal tubule-podocyte cells (**Fig. 5J,K)**. LTL+ proximal tubule segments were also observed more frequently, suggesting that retinoic acid indeed has a similar proximalizing effect here as in the zebrafish. These data indicate that retinoic acid signaling may increase progenitor exit from the SIX2+ state, restrict the spatial scale of Wnt-induced differentiation and promote an appropriate bias of fates during subsequent nephron segmentation. Together these data explain how a consistent Wnt/β-catenin signal *in vivo* may be differentially interpreted by nephron progenitors due to rhythmic YAP and retinoic acid signaling dynamics over the branching morphogenesis life-cycle, setting appropriate renewal vs. differentiation balance and segment bias.

Discussion

Our data together reveal that the nephrogenic niche alternates between renewal and differentiation phases in synchrony with the ureteric bud branching program local to each niche. We validated several hits at the protein level, especially downstream of Wnt signaling, that are crucial to nephron progenitor commitment to early nephron stages. The data provide molecular-level insight into our previous inference that nephrogenesis pauses early in each branching cycle[29]. We also show that incorporation of rhythmic signaling in human iPSC-derived nephron progenitor organoids may aid synthetic control over renewal vs. differentiation decision-making in contexts removed from native branching morphogenesis, essential to the development of organoids and tissue chips for kidney regenerative medicine.

The data leave several questions open for future study. Firstly, are life-cycle-correlated transcriptional changes contributed by all nephron progenitors equally, or through transitions of progenitors between states? The cap mesenchyme niche has spatial structure, with more naive CITED1+/SIX2+ nephron progenitors sitting closer to the organ surface while primed CITED1-/SIX2+ progenitors reside on the medullary side of ureteric bud tips[23,31]. Paradoxically, nephron progenitors migrate among these sub-compartments[32,33], such that the connection between commitment state and position in the niche is still being formalized[28]. The new rhythmic 'axis' we uncovered adds another tool that could be used to parse single-cell-resolution spatial sequencing data to resolve this.

Second, what is the molecular nature of the pace-maker orchestrating the transcriptional rhythm? Several possibilities remain since the ureteric bud life-cycle accompanies changes in niche size[1], curvature[35], and mechanics[29], all of which could feed back into nephron progenitor decision making by modulating reciprocal morphogen signaling between niche cell compartments. The types and timing of signaling pathways revealed through spatial sequencing also have an intriguing overlap with those operating in the somitogenesis clock. Somites (future vertebral, skeletal muscle and cartilage cells) share morphological features with early nephrons – both involve periodic, fractional commitment of mesoderm-derived cells to discrete structures through

mesenchymal to epithelial transitions. Discrete blocks of presomitic mesoderm cells condense in response to a molecular clock consisting of alternating cycles of Wnt and Notch/FGF-MAPK signaling[71,95]. Our spatial sequencing data show similar alternating Wnt and Notch/FGF cycles in nephron progenitors, including several transcripts previously found to be rhythmically regulated in mouse presomitic mesoderm (e.g. *Hes1*, *Hey1*, *Nkd1*, *Id1*, *Nrarp*, *Ptpn11*, *Bcl9l*, *Tnfrsf19*, and *Phlda1*, see **Fig. S11A**)[71]. A somitogenesis gene set was also enriched in nephron progenitors from pre-branching vs. post-branching niches at $p = 0.1$ (**Fig. S11B**). These data suggest that shared developmental mechanisms may be at play. If so, the role of YAP as a mechanosensitive excitability threshold for oscillations[96] may be transferable to nephrogenesis, perhaps forming a link to our previous discovery of rhythmic mechanical stress in the niche synchronized with branching[29]. The existence of a somitogenesis-like clock operating in nephron progenitors could be tested via lineage-specific reporter systems in explants or mouse primary cell/human iPSC-derived kidney organoids.

An alternative candidate for the pace-maker is suggested by the approximately 24 hr ureteric bud branch doubling time after ~E15, coincident with the emergence of a circadian transcriptional rhythm[97]. However, we did not see a GSEA signature for circadian regulation of gene expression correlated with the branching life-cycle (minimum $p = 0.65$ for niche age category comparisons, **Fig. S11C**). Moreover, since branching is asynchronous among ureteric bud tips it is unlikely that each niche is separately entrained to a different circadian phase.

The rhythmic retinoic acid metabolism and stromal-like nephron progenitor signatures appearing in our data also warrant further investigation. Cyclic retinoic acid metabolism may affect autonomous signaling in nephron progenitors, act as a 'filter' that modulates known stroma-ureteric bud signaling[98], and/or create a gradient involved in somitogenesis-like signaling[99]. Our spatial sequencing and protein-level validation data are consistent with either transient excursions of nephron progenitors through the stromal-like state during differentiation and/or (more likely) increased mixing between nephron progenitor and stromal cell compartments in post-/pre-branching phases. One possibility is that cell biophysical properties change during nephron progenitor priming to disfavor their association with the ureteric bud interface, stabilizing stromal interactions while nephron progenitors condense and undergo MET as they join new nephron aggregates. While requiring validation, this explanation is attractive given the rhythmic variation in cell-cell/cell-matrix adhesion-related transcripts in our cap mesenchyme GeoMx data including *Tnc*, *Itga8*, and *Tgfbi*[36,47,48,50,51,100]. Alternatively or in conjunction, life-cycle-correlated intercalation of stromal cells via protrusion into the niche may confer contact-dependent pro-differentiation signaling in nephron progenitors[20,23,38,52,62,101].

Looking to the future, mimicking rhythmic niche signaling could serve as a strategy to achieve co-existence of nephron progenitor pools and differentiating nephrons, enabling multiple waves of nephrogenesis in a single differentiation experiment. This would ease the lack of ongoing nephrogenesis that has limited the use of human autologous stem-cell derived nephrons in regenerative medicine applications[8].

Acknowledgements

We thank Kieran Short, Lukasz Bugaj, Louis Prahl, Jonathan Levinsohn and Katalin Susztak for helpful suggestions relating to our preliminary data. We thank Kyle McCracken and Pedro Medina for advice on kidney organoid air-liquid interface culture and immunofluorescence, Kate Bennett at the Penn Medicine Center for Molecular Studies In Digestive and Liver Diseases, Molecular Pathology and Imaging Core (MPIC, funded under NIH center grant P30-DK050306) for embryonic kidney sectioning services, Carol Gao and Kenji Yeoh for assistance with organoid culture, and Mei Zhang and Xiaoxu Yang at the Children's Hospital of Philadelphia Single Cell Technology core facility for assistance with GeoMx spatial sequencing assays. This research was partially supported by the NSF through the University of Pennsylvania Materials Research Science and Engineering Center (MRSEC, DMR-2309043). This work was supported by the Predoctoral Training Program in Developmental Biology T32HD083185 (JMV), NIH NIGMS MIRA R35GM133380 (AJH), NIH NIDDK R01DK132296 (AJH), NSF CAREER award 2047271 (AJH), and Penn Center for Precision Engineering for Health (CPE4H) pilot grant (AJH).

Declaration of interests

The authors declare no competing interests.

Methods

Animal experiments. Mouse protocols followed NIH guidelines and were approved by the Institutional Animal Care and Use Committee of the University of Pennsylvania. E17 embryos were collected from timed pregnant CD-1 mice (Charles River) and stages confirmed by limb anatomy as previously described[102]. Embryonic kidneys were dissected in chilled Dulbecco's phosphate buffered saline (DPBS, MT21-31-CV, Corning)[103].

GeoMx digital spatial profiling for whole transcriptome analysis (WTA). The NanoString GeoMx Digital Spatial Profiler (DSP) enables spatially resolved RNA expression measurement[39]. GeoMx DSP analysis was performed according to manufacturer protocols. Freshly dissected E17 mouse kidneys were partially flattened between two 1" x 3" standard microscope slides spaced apart using shims cut from 750 µm-thick plastic (Grainger) and held together using rubber bands during fixation for 2 hr in 4% paraformaldehyde (PFA). Kidneys were then stained with 20 µg ml^{-1} AlexaFluor 488-labeled peanut (*Arachis hypogaea*) agglutinin lectin (PNA, L21409, Sigma) for 1 hr in RNAse-free PBS to mark ureteric bud tubules, followed by 3 x 10 min washes in RNAse-free PBS.

Kidneys were embedded in paraffin and sectioned at 5 µm thickness before mounting sections on a positively charged histology slide[104]. Sections were deparaffinized and rehydrated by heating to 60°C for 15 min followed by 3 x 2 min washes with xylene, 2 x 2 min washes with 100% ethanol, and 1 min washes each in 95%, 80%, and 70% ethanol in deionized (DI) water, followed by 1 min wash in DI water. Antigen retrieval was then achieved by heating sections in 10 mM citrate buffer (pH 6) using a pressure cooker for 15 min, followed by blocking for 30 min at room temperature in 1x PBS + 0.1% BSA + 0.2% Triton X-100. Sections were then stained with anti-SIX2 antibody (1:600, 11562-1-AP, Proteintech, RRID: AB_2189084) in blocking buffer at 4°C overnight, washed 3 x 5 min in PBS + 0.1% Tween-20, incubated with AlexaFluor 647-conjugated donkey anti-rabbit secondary antibody (1:200, A31573, ThermoFisher, RRID: AB_2536183) in blocking buffer at room temperature for 1 hr, and washed 3 x 5 min in PBS + 0.1% Tween-20.

The tissue sections were then hybridized with Mouse WTA probes overnight at 37°C. Sections were subjected to 2 x 25 min washes in 1:1 4x SSC and formamide, and 2 x 5 min washes in 2x SSC. The slide was then loaded onto the GeoMx DSP and scanned. The regions of interest (ROIs) were manually selected using the polygon tool, guided by SIX2 staining. Oligos from the hybridized probes in the ROIs were released using photo-cleaving UV light and collected into a 96-well plate. After drying overnight, samples were resuspended in nuclease-free water. Library preparation was performed according to the manufacturer's instructions. i5 and i7 indexes (unique dual indexes) as well as P5 and P7 sequences were added to the photocleaved oligonucleotides through PCR amplification. PCR products were pooled and purified with two rounds of

AMPure XP beads (Beckman Coulter). The size and purity of the pooled library were assessed using a BioAnalyzer High Sensitivity DNA chip (Agilent technologies). The concentration of the library was measured using the Qubit 4 Fluorometer (Thermo Fisher Scientific). Paired end (2 x 27 bp reads) sequencing was performed on an Illumina NextSeq 2000 instrument using a P2-100 flow-cell with a 5% PhiX spike-in. Reads were aligned to barcodes as previously described[39].

Spatial sequencing data analysis. GeoMx data were analyzed in R using code modified from Bioconductor[105] and NanoStringNCTools, GeomxTools, and GeoMxWorkflows libraries. An extra column containing the qualitative niche age annotations ('pre' = pre-branching, 'mid' = mid-branching, 'post' = post-branching) were appended to the sample annotation files associated with each analysis. DCC files for each ROI (a.k.a. 'segment'), PKC, and modified sample annotation files were loaded and quality control performed by first filtering segments using the following parameters - minimum number of reads per segment (1000), minimum % of reads trimmed (80%), minimum % of reads stitched (80%), minimum % of reads aligned (75%), minimum sequencing saturation (50%), minimum negative control counts (1), maximum counts observed in no template control well (9000), minimum segment area (100). Ratio and global probe quality control was performed according to the vignette. Gene-level count data were generated and filtered to remove regions below LOQ. LOQ was defined as two geometric standard deviations above the geometric mean of negative control probes, or a minimum LOQ of 4. Segments having fewer than 20% of genes detected above LOQ were first filtered out, followed by genes detected in fewer than 20% of segments. Count data were then Q3 normalized before differential expression analysis using a linear model (modelDE.R, Roy Lardenoije) suited to comparing regions within the same slide. FDR values were determined via Benjamini-Hochberg multiple test correction.

The following analyses were also performed in R (RStudio v2023.06.1+524) using the indicated libraries: tSNE (Rtsne), unsupervised clustering of $\log_2$-transformed normalized count data with 'correlation' option (pheatmap), gene expression and volcano plots (ggplot2, ggrepel).

Clustering and non-linear dimensional reduction was performed using Seurat[106]. Briefly, raw GeoMx count data were loaded into R as a Seurat object and log-normalized using the NormalizeData function. The top 500 highly variable features were detected using the FindVariableFeatures function. Data were scaled to mean and variance per gene across ROIs of 0 and 1 respectively. Linear dimensional reduction was performed by principal component analysis using the RunPCA function, taking the first 20 principal components. K-nearest neighbor graph-based clustering with modularity optimization was then performed using FindNeighbors and FindClusters. tSNE was then performed using RunTSNE with a perplexity of 14 (based on 43 ROIs in our experiment).

Kidney immunofluorescence imaging. Immunofluorescence staining and imaging was performed as previously described[107], using protocols adapted from Combes *et al.* and O'Brien *et al.*[36,108]. Briefly, dissected kidneys were fixed in ice cold 4% paraformaldehyde in DPBS for 20 min, washed three times for 5 min per wash in ice cold DPBS, blocked for 2 hr at room temperature in PBSTX (DPBS + 0.1% Triton X- 100) containing 5% donkey serum (D9663, Sigma), incubated in primary and then secondary antibodies in blocking buffer for at least 48 hr at 4°C, alternating with 3 washes in PBSTX totaling 12-24 hours. The minimum duration of primary and secondary antibody incubations and washes depended on the age of the kidney, as previously described[108].

Primary antibodies and dilutions included rabbit anti-SIX2 (1:600, 11562-1-AP, Proteintech, RRID: AB_2189084), goat anti-ITGA8 (1:20, AF4076, R&D, RRID: AB_2296280), mouse anti-E-cadherin (1:50, clone 34, 610404, BD Biosciences, RRID: AB_397787), Goat anti-PDGFRA (1:500, AF1062, R&D Systems, RRID:AB_2236897), rabbit anti-phospho-Smad1/5 (1:800, 9516, Cell Signaling Technology, RRID:AB_491015), rabbit anti-Ki67 (0.5 µg/ml, ab15580, Abcam, RRID:AB_443209), mouse anti-MEIS1/2/3 (0.5 µg/ml, 39795, Active Motif, RRID:AB_2750570), rabbit anti-DHRS3 (1:500, 15393-1-AP, Proteintech, RRID:AB_2091855), rabbit anti-CELSR1 (1:500, ABT119, Millipore, RRID:AB_11215810), rabbit anti-Cyclin D1 (1:200, ab16663, Abcam, RRID:AB_443423), rabbit anti-MUCL1 (1:200, PA5-58653, ThermoFisher, RRID: AB_2644299), rabbit anti-RETSAT (1:350, PA5-65443, ThermoFisher, RRID: AB_2663683), rabbit anti-TTC28 (1:200, ab197076, Abcam), rabbit anti-PAX8 (1:250, 10336-1-AP, Proteintech, RRID: AB_2236705), rabbit

anti-LEF1 (1:300, 2230, Cell Signaling Technology, RRID: AB_823558), rabbit anti-MRPS17 (1:200, 18881-1-AP, Proteintech, RRID: AB_10597844), rabbit anti-FGF1 (1:200, ab9588, Abcam, RRID: AB_308729), rabbit anti-LTBP1 (1:200, ab78294, Abcam, RRID:AB_1952060), and goat anti-JAG1 (1:150, AF599, R&D Systems, RRID: AB_2128257). Secondary antibodies (all raised in donkey) were used at 1:300 dilution and included anti-rabbit AlexaFluor 647 (A31573, ThermoFisher, RRID: AB_2536183), anti-rabbit AlexaFluor 555 (A31570, ThermoFisher, RRID: AB_2536180), anti-rabbit AlexaFluor 488 (A21206, ThermoFisher, RRID: AB_2535792), anti-mouse AlexaFluor 555 (A31572, ThermoFisher, RRID: AB_162543), and anti-goat AlexaFluor 488 (A11055, ThermoFisher, RRID: AB_2534102). In some experiments, samples were counterstained in 300 nM DAPI (4',6-diamidino-2-phenylindole; D1306, ThermoFisher), and/or 20 µg ml^{-1} AlexaFluor 488-labeled peanut (*Arachis hypogaea*) agglutinin lectin (PNA, L21409, Sigma) diluted in blocking buffer for 2 hours at room temperature, followed by 3 washes in PBS.

Kidneys were imaged in wells created with a 2 mm diameter biopsy punch in a ~5 mm-thick layer of 15:1 (base:crosslinker) polydimethylsiloxane (PDMS) elastomer (Sylgard 184, 2065622, Ellsworth Adhesives) set in 35 mm coverslip-bottom dishes (FD35-100, World Precision Instruments). Imaging was performed using a Nikon Ti2-E microscope equipped with a CSU-W1 spinning disk (Yokogawa), a white light LED, laser illumination (100 mW 405, 488, and 561 nm lasers and a 75 mW 640 nm laser), a Prime 95B back-illuminated sCMOS camera (Photometrics), motorized stage, 4x/0.2 NA, 10x/0.25 NA, 20x/0.5 NA, and 40x/0.9 NA lenses (Nikon), and a stagetop environmental enclosure (OkoLabs).

Average immunofluorescence was quantified for cap mesenchyme regions of interest segmented using Ilastik[109] v1.4.1b6. Segmented outlines were manually refined in FIJI as required.

HCR RNA-FISH. E17 mouse embryonic kidneys dissected in RNase-free PBS were assayed by whole-mount hybridization chain reaction (HCR v3.0) single-molecule RNA fluorescence in-situ hybridization (smFISH) similar to published protocols[42,110–113]. Probe sets were designed using in-house software (AnglerLite) and are provided in **Supplementary Files**). Buffers and hairpin solutions were procured from Molecular Instruments, Inc. Kidneys were transferred to 1.5 ml Eppendorf tubes and fixed in 4% PFA overnight at 4°C. Kidneys were washed 3 x 5 min in PBST and dehydrated on ice by serial 10 min incubations in 25%, 50%, 75%, and 100% methanol:PBST washes before incubation at -20°C for > 16 hr. Kidneys were rehydrated on ice by serial 10 min incubations in 25%, 50%, 75%, and 100% PBST:methanol, followed by one 10 min PBST wash at room temperature. Kidneys were further permeabilized for 1 hr in 2% SDS, 10 µg/ml proteinase K in PBST. Kidneys were washed 3 x 5 min in PBST, post-fixed 20 min in 4% PFA at room temperature, washed 5 x 5 min in PBST, and incubated in probe hybridization buffer for 5 min. Kidneys were pre-hybridized with pre-warmed probe hybridization buffer for 30 min at 37°C. 100 µl of 16 nM probe solution was then prepared from a 1 µM stock and pre-warmed to 37°C for 15 min before probing kidneys overnight (>12 hr) at 37°C. Probe wash buffer was pre-heated to 37°C and used to wash kidneys for 4 x 30 min at 37°C, followed by 2 x washes with 5x sodium chloride-sodium citrate buffer tween buffer (SSCT) at room temperature. Amplification buffer was equilibrated at room temperature while 2 µl of 3 µM stocks of hairpins 1 and 2 were snap-cooled from 95°C for 90s to 20°C for 30 min in the dark. Kidneys were incubated with pre-warmed amplification buffer for 30 min at room temperature before incubating with 100 µl amplification buffer containing 50x dilutions of each hairpin at room temperature overnight (12-16 hr). Excess hairpins were removed by washing in 5x SSCT at room temperature 2 x 5 min, 2 x 20 min, and 1 x 5 min, followed by 3 x 5 min washes in PBST.

Kidneys were imaged by confocal fluorescence microscopy at 20x and 40x as for antibody assays (see **Kidney immunofluorescence imaging.**)

Human iPSC-derived nephron progenitors. Nephron progenitor cell 'puck' organoids were generated from $SIX2^{EGFP}$ transgenic reporter iPSC line (*SIX2*-T2A-*EGFP*, Murdoch Children's Research Institute / Kidney Translational Research Center, Washington University Nephrology) and $MAFB^{BFP}$;$GATA3^{mCherry}$ transgenic reporter iPSC line[114] according to published protocols[78,79,115]. Briefly, iPSCs were maintained in standard tissue-culture treated 6-well plates in stem cell maintenance medium plus supplement (mTeSR+ kit, StemCell Technologies 100-0276). Cells were passaged using Accutase (StemCell Technologies, 07920) and plated at a density of 5,200 cells/cm^2. Differentiation was induced with TeSR-E6 Medium plus supplements (TeSR-E6+)

(STEMCELL Technologies 05946) and 7μM CHIR 99021 (Tocris, 4423) the following day, and media was refreshed every other day. On day 5, wells were washed with DPBS and media was changed to TeSR-E6+, 1 μg/ml heparin (Sigma-Aldrich H4784) and 200 ng/ml FGF9 (R&D Systems 273-F9-025). Media was refreshed every day. On day 10, cells were lifted using Accutase and TeSR-E6+ was used to quench digestion. Cells were resuspended in TeSR-E6+ and counted, centrifuged at 300g for 3 min and resuspended in the residual media volume remaining after aspiration of TeSR-E6+ to create a dense cell slurry at ~0.3 x 10^6 cells/μl. 1 μl aliquots of the slurry were then spotted onto 6-well 0.4 μm polyester transwell membranes (CellTreat, 230607) overlying TeSR-E6+ and 7μM CHIR 99021 'pulse' media for 2 hr, which was then exchanged for 'chase' media consisting of TeSR-E6+, 1 μg/ml heparin, and 200 ng/ml FGF9. For select conditions, the CHIR pulse was combined (in pulse media) or staggered (in chase media) with 0.1 μM TTNPB (Tocris 0761), 4 μM TRULI (MedChem Express HY-138489 or Sigma-Aldrich SML3634), or equivolume DMSO. In these cases, wells were then washed with DPBS before changing to chase media. Media was refreshed the following day. On day 12, transwells were exchanged with DPBS and media switched to TeSRE6+. Media was refreshed every other day until reaching the experiment endpoint.

Organoid immunofluorescence. Organoids were fixed in 4% paraformaldehyde for 15 min. Fixed cells were then washed twice for 10 min in PBSG (DPBS + 7.5 g/L glycine) and once in DPBS. Organoids were permeabilized in 0.5% Triton-X-100 for 30 min at room temperature and blocked for 1hr at room temperature in IF Wash (DPBS + 1g/l Bovine Serum Albumin + 0.2% Triton-X-100 + 0.04% Tween-20) + 10% donkey serum. Organoids were then incubated overnight at 4°C in appropriate dilution of primary antibody in IF Wash + 10% donkey serum, washed three times for 1 hour in IF wash at room temperature, and incubated in secondary antibody at overnight at 4°C in IF wash + 10% donkey serum. Organoids were again washed three times in IF wash for 1 hour. Organoids were counterstained in 1 μg/ml DAPI in DPBS and washed once in DPBS before imaging using confocal microscopy (see **Kidney immunofluorescence imaging)**. Primary antibodies and dilutions were rabbit anti-SIX2 (1:400, 11562-1-AP, Proteintech, RRID: AB_2189084), rabbit anti-ECAD (1:300, 3195, Cell Signaling Technology, RRID: AB_2291471), goat anti-JAG1 (1:150, AF599, R&D Systems, RRID: AB_2128257), goat anti-GATA3 (1:20, AF2605, R&D Systems, RRID: AB_2108571), sheep anti-NPHS1 (1:40, AF4269, R&D Systems, RRID: AB_2154851), and biotinylated LTL (1:300, B-1325-2, Vector Laboratories). Donkey secondary antibodies were used at 1:300 dilution: anti-rabbit AlexaFluor 647 (A31573, ThermoFisher, RRID: AB_2536183), anti-goat AlexaFluor 488 (A11055, ThermoFisher, RRID: AB_2534102), anti-sheep AlexaFluor 555 (A21436, ThermoFisher, RRID: AB_2535857), and DyLight 405-Streptavidin (016-470-084, Jackson ImmunoResearch).

For day 12 organoids, nephron progenitor (SIX2+) and early nephron (JAG1+) % area relative to DAPI+ area was determined by thresholding *z*-stack montages in FIJI. For day 25 organoids, glomeruli (NPHS1+) % area was determined by thresholding *z*-stack montages while proximal tubule (LTL+) % area, distal tubule (only ECAD+) % area, and connecting segment (nuclear GATA3+ and ECAD+) % area relative to organoid area (determined by manual annotation of background signal) were determined by manual annotation of z-stack montages followed by thresholding. Analyses were performed on a single, central z-plane for each organoid.

Organoid RNA isolation and quantitative PCR. Organoids were collected 8 hours after seeding for RNA extraction with 8 organoids pooled for each condition. Following the manufacturer protocols, we used the RNeasy Mini Kit (Qiagen 74104) to isolate RNA and the High-Capacity RNA-to-cDNA Kit (Applied Biosystems 4387406) to generate cDNA libraries. For qPCR, we used the PowerUp SYBR Green Master Mix (Applied Biosystems A25742). We used an Applied Biosystems 7300 thermocycler set to manufacturer suggested times and temperatures for PowerUp SYBR Green Master Mix. 25 ng of cDNA were used in each reaction along with the appropriate qPCR primers at 500 nM. qPCR primers for *CRABP2*, *CTGF*, *CYP26A1*, *CYR61*, *GAPDH*, *HPRT*, and *RARB* were used (**Table S2**). DeltaDeltaCt values were calculated using either *GAPDH* or *HPRT* as housekeeping genes. Samples were run in triplicate for qPCR analysis.

scRNA-seq data analysis. Gene expression matrices generated from scRNA-seq of dissociated E15.5 mouse embryonic kidneys in Lawlor *et al.* were used[32]. These matrices were accessed from the Gene Expression Omnibus (GEO, NCBI) under accession code GSE118486 and sample mk1 was used for further analysis. Analysis was done similarly to Lawlor *et al.* In short, the Seurat library[116,117] was used to import the gene

expression matrix to R and for downstream analyses. Cells with less than 200 genes expressed or with greater than 7.5% mitochondrial gene expression were removed. Genes expressed in less than 3 cells were removed from the dataset. The filtered dataset contained 2,708 cells with an average of 2,441 unique genes detected per cell. Cell cycle scoring was done using the CellCycleScoring function. Scaled data matrices were then generated using the ScaleData function. Shared nearest neighbor (SNN) clustering was performed for whole kidney data using resolution 0.5 for the first 15 principal components calculated from a set of 2,000 variable genes. Differentially expressed marker genes were identified using a Wilcoxon rank sum test and compared to the published list of marker genes from Lawlor *et al.*[32] to assign cell identity. SNN clustering was then performed on cells belonging to the nephron lineage clusters using resolution 0.5 for the first 12 principal components calculated from a set of 2,000 variable genes. Again, differentially expressed marker genes were identified in Seurat using Wilcoxon rank sum test and compared to a list of marker genes for distinct nephron lineage clusters published by Lawlor *et al.*[32] to assign cell identity. Fold-change and Wilcoxon rank sum *p*-value for individual genes in volcano plots were calculated by comparing the committing cluster to the progenitor cell clusters. A list of 171 highly upregulated genes in the committing cluster compared to the progenitor cell cluster was generated by taking genes with $\log_2$(fold-change) of at least 0.25 and Bonferroni corrected adjusted Wilcoxon rank sum test *p*-value less than 0.05 between the clusters.

To gain higher resolution in cell types, gene expression matrices generated from scRNA-seq of dissociated E18.5 mouse embryonic kidneys in Combes *et al.* were used[47]. These matrices were accessed from the Gene Expression Omnibus (GEO, NCBI) under accession code GSE108291 and samples E18.5 kidney 1 through 3 were used for further analysis. Analysis was done similarly to Combes *et al.* In short, the Seurat library[116,117] was used to import the gene expression matrix to R and for downstream analyses. Cells with less than 200 genes expressed, greater than 95% of genes with zero assigned reads, greater than 4,500 transcript counts, or greater than 6.5% mitochondrial gene expression were removed. Genes expressed in less than 3 cells, mitochondrial and ribosomal genes, and genes without annotations were removed from the dataset. The filtered dataset consisted of 5,494 cells and 15,747 genes, with an average of 2,383 unique genes detected per cell. Cell cycle scoring was done using the CellCycleScoring function, and the filtered dataset was normalized regressing out factors related to cell cycle using the NormalizeData function. Scaled data matrices were then generated using the ScaleData function. Shared nearest neighbor (SNN) clustering was performed for whole kidney data using resolution 0.8 for the first 30 principal components calculated from a set of 2,000 variable genes. Differentially expressed marker genes were identified using a Wilcoxon rank sum test and compared to the published list of marker genes from Combes *et al.*[47] to assign cluster identity. Clusters with similar marker profiles were combined for plotting, achieving a similar set to those reported by Combes. However, we did not recover a unique K14 NP-STR cluster and we recovered the extra clusters K1,2,4 STR (with stromal markers that overlapped K1 STR-CD, K2 STR-CS, and K4 STR-MS), and K3,9 UE/CnS (with markers that overlapped K3 DN and K9 UE). SNN re-clustering was then performed on cells belonging to the nephron lineage clusters (K0 NP, K3 DN, K6 SSB, K7 RV, K5 EPT, K8 PT, K3,9 CnS, K12 PTA, K15 Pod) using resolution 0.8 for the first 35 principal components calculated from a set of 2,000 variable genes. Again, differentially expressed marker genes were identified in Seurat using Wilcoxon rank sum test and compared to a list of marker genes for distinct nephron lineage clusters published by Combes *et al.*[47] to assign cell identity. Again, we recovered a similar cluster set to those reported by Combes. However, we did not recover a unique N10 NP-STR cluster (instead we found this was a sub-cluster of N6 NP based on *Col3a1* expression, which was identified as a marker in Combes), or a unique N12 CnS cluster (we found this to be combined with N8 distal SSB in our analysis).

Gene Set Enrichment Analysis (GSEA). Gene set enrichment plots were generated using GSEA desktop software[46] from Q3-normalized GeoMx gene count data. Gene sets consisted of the above differentially expressed set for committing:naive nephron progenitors (see **Fig. 3D**) and others available in the Broad Institute's Molecular Signatures Database (MSigDB, **Fig. 3C**). FDR q-values < 0.25 were considered to be significant per the GSEA user guide[118].

Rendering and graphics. 3D reconstruction of E14 kidney in Fig. 1 was generated using ImarisViewer v10.0.1 (Oxford Instruments). Insets were generated by exporting surface .stl files from FIJI 3D viewer and

rendering in Rhino 7 (Robert McNeel & Associates). Cartoon schematics with 3D effects were generated in Rhino using Grasshopper and Kangaroo (Daniel Piker) packages.

Statistical analysis. One-way analysis of variance (ANOVA) with correction for multiple comparisons using Tukey's honestly significant difference test was performed in MATLAB using anova1.m and multcompare.m functions.

Supplementary Information

Supplementary Notes

Note S1. All-gene analysis hits. *Retsat* codes for the enzyme retinol saturase, which metabolizes the retinoic acid substrate all-trans-retinol, potentially reducing its availability for the synthesis of retinoic acid (RA)[119,120]. RA produced by stromal cells is required to induce RET expression in the ureteric bud, a receptor tyrosine kinase crucial to branching morphogenesis[98,121]. While retinoic acid signaling is essential for zebrafish renal progenitor differentiation[91], its role in mammalian nephron progenitors is less clear[92]. While limited in its functional characterization, *Mucl1* codes for a small glycoprotein in the mucin family[122]. Muc-like 1 is a breast cancer metastasis marker and drove β-catenin activation and cell invasion/migration in human colorectal cancer cell lines[43]. It was also proposed to drive cell cycle progression by activating focal adhesion kinase (FAK)/Jun kinase (JNK) signaling in breast cancer cell lines[123], reminiscent of similar signaling activities of the mucin MUC1[124].

Note S2. Considerations for GeoMx differential expression analysis. We expected *a priori* that differential expression analysis would have limited statistical power due to the limited dynamic range of the GeoMx assay[125], subtle expected differences between nephron progenitor populations (relative to a similar analysis between distinct cell lineages), the limited ROI number able to be captured in a single tissue slice, and the temporal continuity between pre-, mid-, and post-branching categories (i.e. the post-branch category blends back into the pre-branch category, etc.). These factors motivated a focus on gene-set enrichment analysis over techniques relying on individual significantly differentially expressed genes.

Note S3. GSEA hits. Several of the most enriched Wnt *pathway* genes in post-branching niches are putative or known antagonists of Wnt signaling, namely the Groucho-related Wnt co-repressor *Tle1*[34,126], *Smad4*[127] and *Ctbp1*[34] (**Fig. S3B**), while several of the most enriched Wnt *target* genes are later[17,25] Notch-relevant transcripts including *Numb*[128], *Maml1*[129], *Adam17*[130], and *Hey1*[25] (**Fig. S3C**). This suggests that Wnt/β-catenin activity is likely higher in nephron progenitors in pre-/mid-branching niches (as further evidenced by their higher expression of the early[25] Wnt targets *Lef1*†, *Pax8*†, and *Ccnd1*† (Cyclin D1)[15,18,58,131], **Fig. S3B,C**, **Fig. 3E, Fig. S5**). The same may be true for retinoic acid signaling, since two of the higher enriched genes in post-branching niches (*Retsat* and *Dhrs3*†) encode enzymes that would act to reduce all-trans RA levels[119,120,132] and the tell-tale retinoic acid target *Rarb*[133–135] is the most enriched of the set in pre-/mid-branching niches (**Fig. S3A**).

Hippo signaling transcripts were enriched in mid-branching relative to post-branching niches (**Fig. S3E**). These enriched transcripts were a mixture of those associated with positive (*Pja2*) and negative (*Stk4*, *Nf2, Wwc1*) effects on YAP signaling.

Note S4. Curated gene list analysis hits (Fig. S5). *Fgf1*† and its receptors *Fgfr1/2* were enriched in nephron progenitors from mid- and post-branching ureteric bud tips. *Fgf1* is expressed in the cap mesenchyme and FGF1 promotes renewal of naive CITED1+ nephron progenitors in mouse primary nephrogenic zone cell cultures[10]. Out-of-phase differential expression of *Fgf1* and *Retsat* is intriguing given the antagonistic interaction between FGF and RA signaling pathways in other developmental contexts, such as somitogenesis, mouse forelimb budding, and distal lung development[136–141]. A similar antagonism between FGF and Wnt signaling may be at play, since *Gas1* was enriched in post-branching niches; *Gas1* is repressed by Wnt signaling in nephron progenitors[17] and otherwise maintains nephron progenitors by sensitizing them to FGF proliferation signaling[65]. Also of note was *Mycn*, enriched in mid-/post-branching niches. N-Myc has been found to cooperate with β-catenin signaling downstream of nephron progenitor renewal signaling via Wnt9b/β-catenin (low)[53]. Other genes with potential life-cycle dependence include the TGFβ superfamily members or associated genes *Bmp7* in mid-branching niches (involved in nephron progenitor proliferation[24] and priming[23]) and *Tgfbi* in post-branching niches (a secreted collagen-associated protein thought to interact with the ECM[51,68]); and the Yap-dependent genes *Traf1* and *Capn6* in post-branching niches (thought to be involved in microtubule and actin cytoskeletal organization)[19,142]. Together with the Hippo GSEA data (**Note S3**, **Fig. S3E**) these data suggest that YAP activity is likely higher in nephron progenitors in post-branching niches - Yap signaling is required for nephron progenitor renewal[19,20,84].

Note S5. Mapping rhythmic hits to progenitor/nephron sub-populations indicates a shift between renewing and differentiating progenitor states, and likely rhythmic stromal cell intercalation into the niche. We went back to the Lawlor *et al.* 2019 E15.5 scRNA-seq clusters to determine which cell types expressed rhythmic hits from the all-gene and curated-gene differential expression analyses. On average, hits associated with pre-/mid-branching niches (e.g. *Ccnd1*, *Lef1*, *Pax8*, *Ltbp1*, *Mycn*, *Fgfr2*) were primarily found in committing nephron progenitors, while hits associated with post-branching niches (e.g. *Stox2*, *Ttc28*, *Fgf1*, *Tnc*, *Pdgfra*†, *Tgfbi*, *Gas1*, *Mest, Eya1*) were primarily found in nephron progenitors and nephron progenitors having a *Pdgfra*+ *Meis1*+ stromal-like signature (**Fig. S6**). Together these data suggest that the expression level or proportion of nephron progenitor, stromal-like nephron progenitor, and committing populations in the cap mesenchyme change over the branching life-cycle.

The validity of the stromal-like population is a matter of debate[47]. Expression of the canonical nephron progenitor markers *Cited1* and *Six2* was slightly higher in the nephron progenitor cluster relative to the stromal-like nephron progenitor cluster, suggesting that, if bona fide, the latter may be an intermediate commitment state. This is supported by our clustering analysis of the Combes *et al.* 2019 E18.5 dataset, which placed their *Col3a1*+ stromal-like population as a subcluster within the N6 committing nephron progenitor cluster (**Fig. 3F**). Transcriptional expression of stromal markers (e.g. *Meis1*, *Pdgfra*, *Foxd1*) has been previously observed in nephron progenitors[32,47,66,73,74], though protein-level expression has been reported to be more rare[73] (and for *Pdgfra*, transcriptional expression has been argued to result from a technical artifact[47]). Nonetheless, we verified positive, heterogeneous MEIS1 and PDGFRA staining in SIX2+ nephron progenitors, including MEIS1-high and PDGFRA+ sub-populations via whole-mount immunostaining (**Fig. S6**). The MEIS1 result agrees with a recent report[74] (but contrasts with another that observed this only in human[75]).

Thus the staining data do appear to validate the presence of rare stromal-like nephron progenitors in the cap mesenchyme. However, these positive cells accompanied but were distinct from stromal cell protrusions that frequently spanned the nephron progenitor compartment, contacting the basal ureteric bud interface (**Fig. S6**). It is likely then that differential stromal cell intercalation by protrusion/mixing into the cap mesenchyme over the branching cycle makes some contribution (potentially almost all of the contribution) to both the spatial and single-cell transcriptional signatures here. This would occur through differential contamination by nephron progenitor-stromal cell doublets in the latter[47]. Indeed, the stromal-like nephron progenitor population is much smaller as a proportion of all nephron progenitors in the E18.5 scRNA-seq data in Combes *et al.* 2019, and *Pdgfra* expression is very sparse relative to the Lawlor dataset, suggesting that this population arises at least in part from technical differences in e.g. tissue dissociation between experiments or kidney stages. In summary, rhythmic stromal gene hits such as *Pdgfra* detected by GeoMx may be reporting on rhythmic expression/proportion of stromal-like nephron progenitors, rhythmic stromal cell intercalation into the niche, or both. We believe that rhythmic stromal cell intercalation into the niche is more likely the dominant contributor overall.

Note S6. LEF1 validation. LEF1+ nephron progenitors are only occasionally seen in the mouse cap mesenchyme but more extensively in human, potentially due to more rapid relocation of these cells to pre-tubular aggregates in mouse[64]. Mugford *et al.* previously saw LEF1+ cells in ureteric bud clefts and ascribed them to a sub-population of cortical interstitial progenitors based on positive staining for LEF1 in *Foxd1* lineage-traced cells[31]. However, *Foxd1* expression also occurs in nephron progenitors and committing cells[32,47], leaving open the possibility of a nephron progenitor origin.

Supplementary Figures

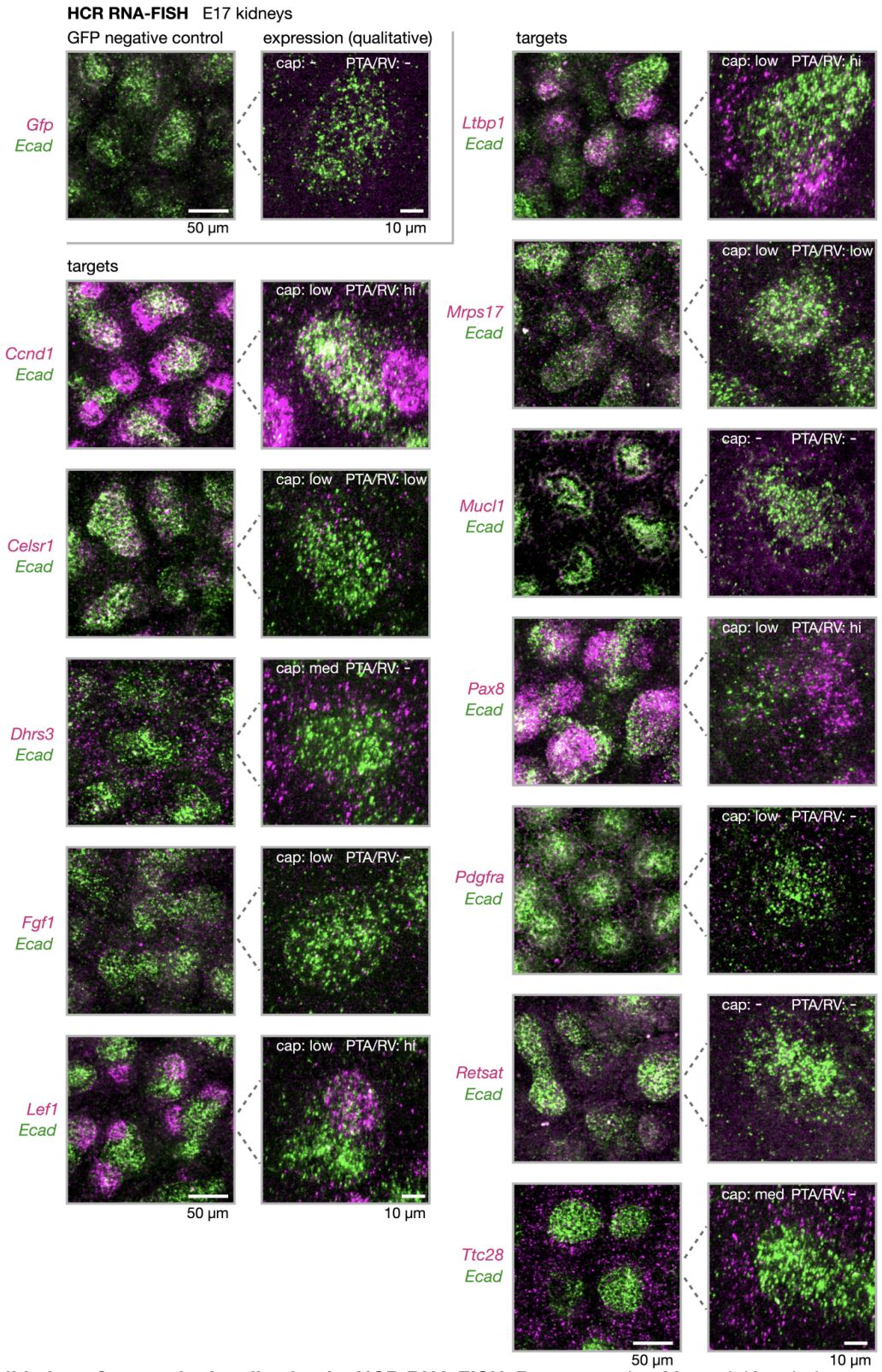

Fig. S1: Validation of transcript localization by HCR RNA-FISH. Representative 20x and 40x whole-mount confocal fluorescence micrographs of E17 kidneys at approximate mid-planes of ureteric bud epithelial tips and surrounding nephrogenic niches. Qualitative expression levels in cap mesenchyme ('cap') and pre-tubular aggregates/renal vesicles ('PTA/RV') are noted, relative to *Gfp* negative control, listed as low, medium (med), high (hi), or no expression observed using the chosen probe set (-). Note that *Mucl1* and *Retsat* were not detected with the chosen probe sets.

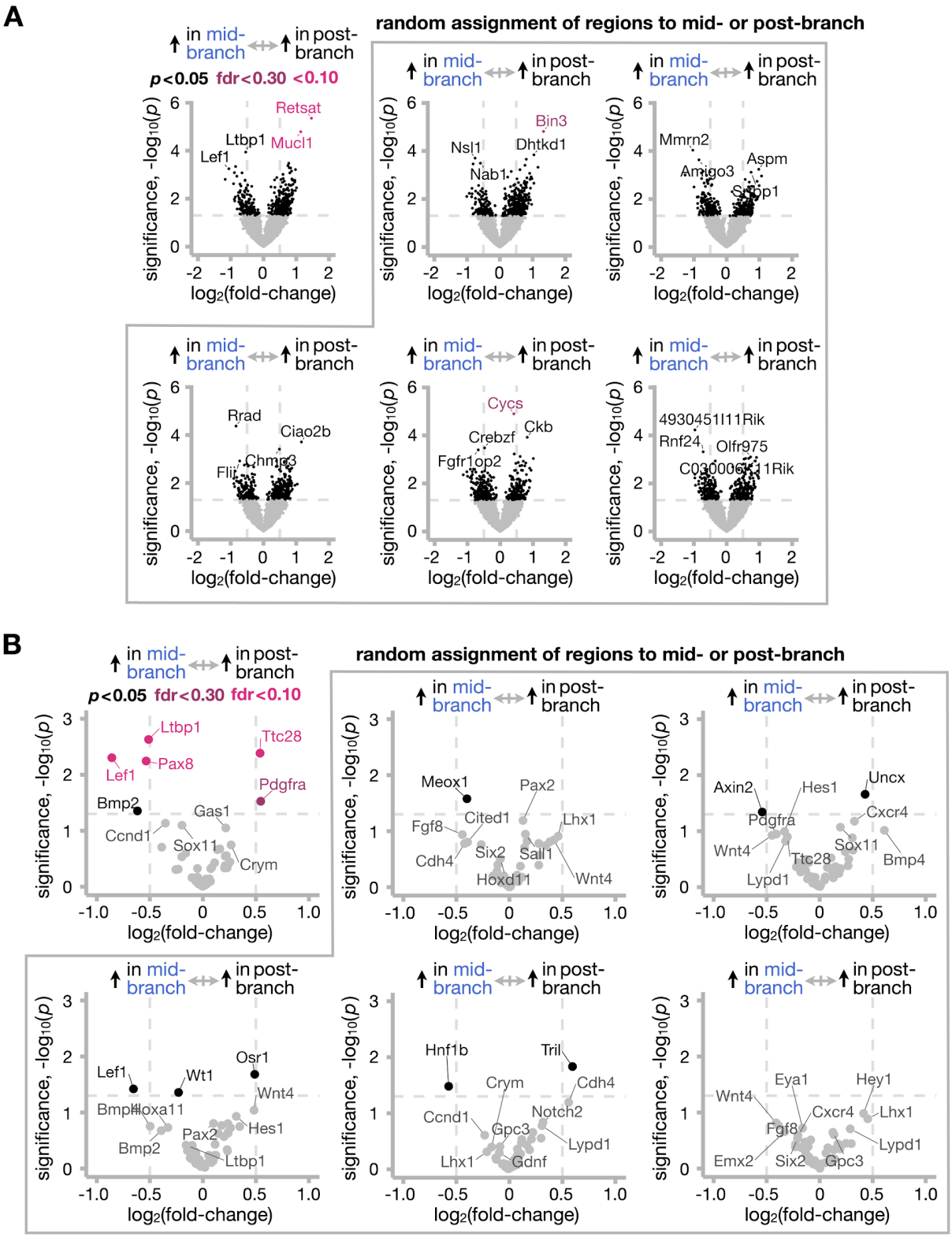

Fig. S2: Hit detection by differential expression analysis is robust to randomized ROI labeling. (**A**) Volcano plots for an example all-gene differential expression analysis with correct assignment of ROIs to niche life-cycle 'age' categories (top left), and five sham cases where ROI assignments were randomized. (**B**) Similar plots for an example curated-gene differential expression analysis.

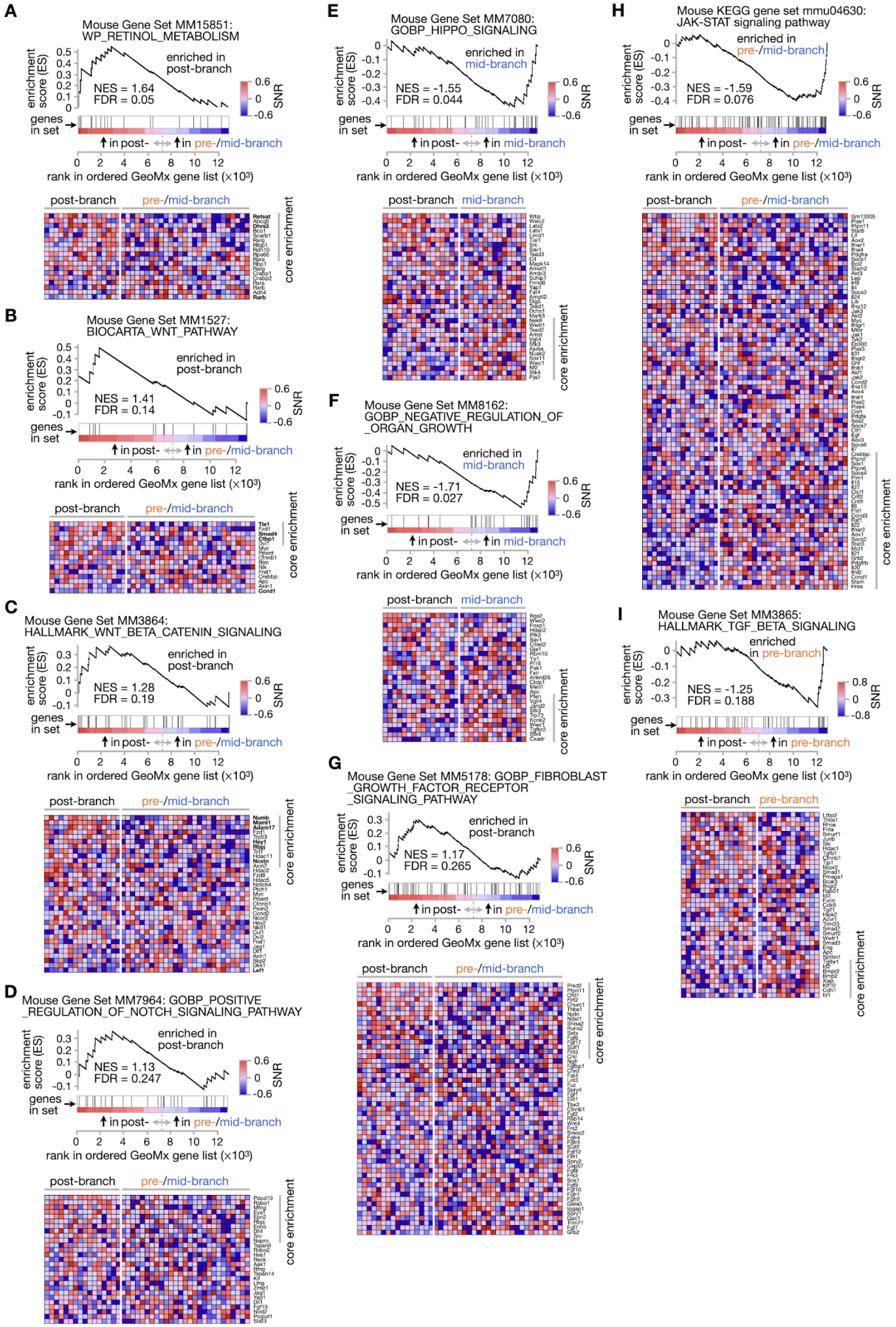

Fig. S3: Full GeoMx gene-set enrichment analyses (GSEA). (**A-I**) Gene set enrichment score plots, 'ticker-tape' plots showing gene rankings in GeoMx transcriptome, and expression heat-maps ordered by gene rank. Comparisons shown are between niche life-cycle 'age' categories with lowest GSEA false-discovery rate (FDR) and/or favoring comparison of one category to the others ('vs. rest') when FDR < 0.05. NES, normalized enrichment score.

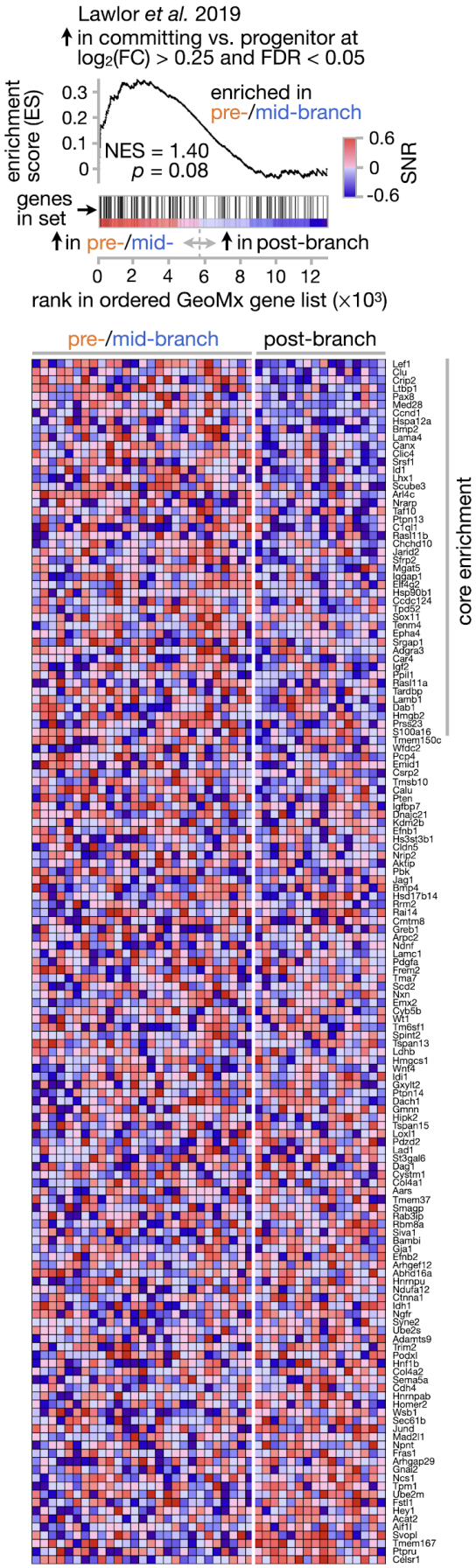

Fig. S4: Enrichment of 'committing' nephron progenitor signature in pre-/mid-branching cap mesenchyme niches. Full GeoMx GSEA results for a gene set created from those differentially expressed in 'committing' nephron progenitors vs. nephron progenitors based on data from Lawlor et al. 2019. Gene set enrichment score plot, 'ticker-tape' plot showing gene rankings in GeoMx transcriptome, and expression heat-map ordered by gene rank. NES, normalized enrichment score.

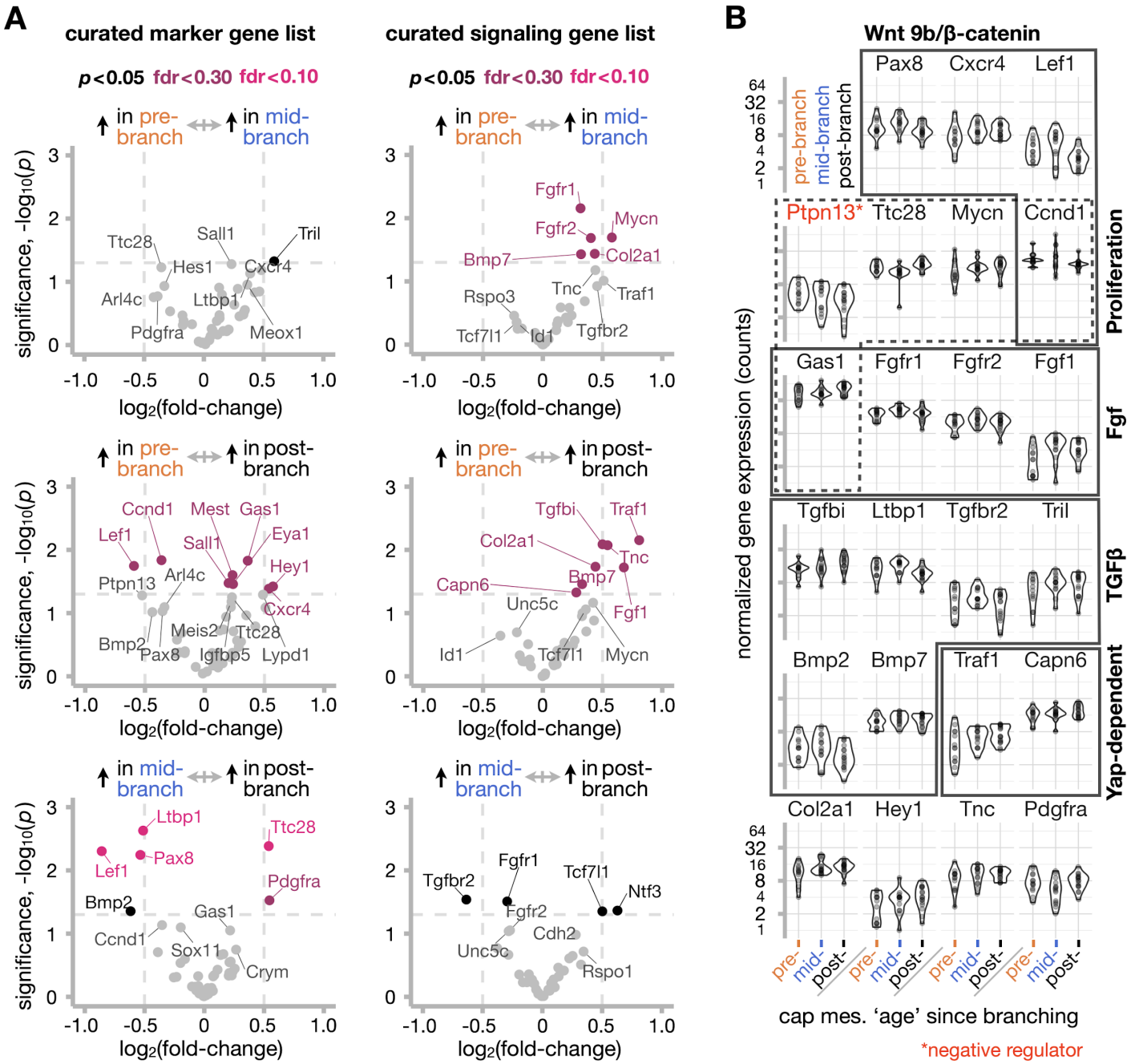

Fig. S5. Differential GeoMx transcript expression analysis between niches in pre-, mid-, and post-branching 'age' categories for curated marker and signaling gene lists. (**A**) Volcano plots for curated marker and signaling gene differential expression analyses between each pair of niche 'age' groups. (**B**) Gene expression plots for a range of hits (typically having FDR < 0.3), grouped by signaling pathway or process (see main text for literature citations). Points represent individual ROIs (cap mesenchyme niches).

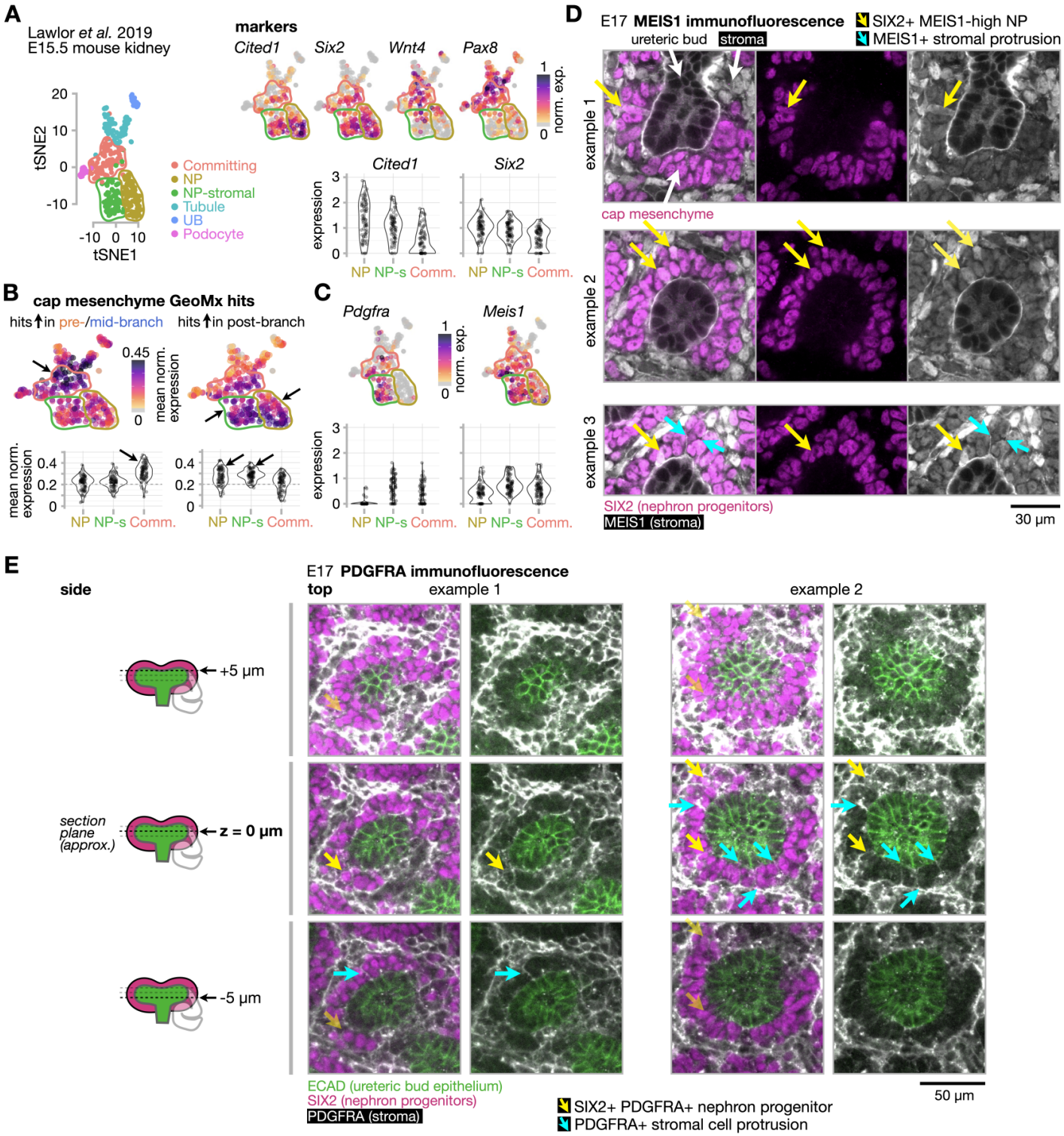

Fig. S6. Mapping rhythmic GeoMx hits to Lawlor *et al.* 2019 scRNA-seq clusters, validation of MEIS1+ and PDGFRA+ SIX2+ stromal-signature nephron progenitors, and observation of stromal cell protrusions into the cap mesenchyme. (**A**) tSNE plots of E15.5 mouse kidney scRNA-seq data from Lawlor *et al.* 2019 showing: *left*, Cell type annotations (NP: nephron progenitor, UB: ureteric bud); *top right*, Feature plots of nephron progenitor (*Cited1*, *Six2*) and differentiation (*Wnt4*, *Pax8*) markers. *Bottom right*, Violin plots of *Cited1* and *Six2* expression by cell type (NP-s: stromal-like nephron progenitors, Comm.: committing nephron progenitors). (**B**) *Top*, Mean normalized expression in Lawlor scRNA-seq clusters of rhythmic GeoMx hits from **Fig. 3E** upregulated in pre-/mid-branching niches and post-branching niches. *Bottom*, Violin plots of the same data by cell type. (**C**) Feature and violin plots of *Pdgfra* and *Meis1* stromal markers. (**D**) Whole-mount confocal immunofluorescence micrograph of E17 mouse kidney to assay for MEIS1 staining in cap mesenchyme (nephron progenitors). Composites (*left*) and individual fluorescence channels (*middle* and *right*) show examples of SIX2+ MEIS1-high nephron progenitors (yellow arrows) and also MEIS1 in stromal cell protrusions into the cap mesenchyme (cyan arrows). (**E**) Similar whole-mount confocal immunofluorescence data for PDGFRA in E17 mouse kidney at ~niche mid-plane and at +/-5 µm in *z* showing PDGFRA protein-level expression in a rare sub-population of SIX2+ cells (yellow arrows) and also in stromal cell protrusions into the cap mesenchyme (cyan arrows).

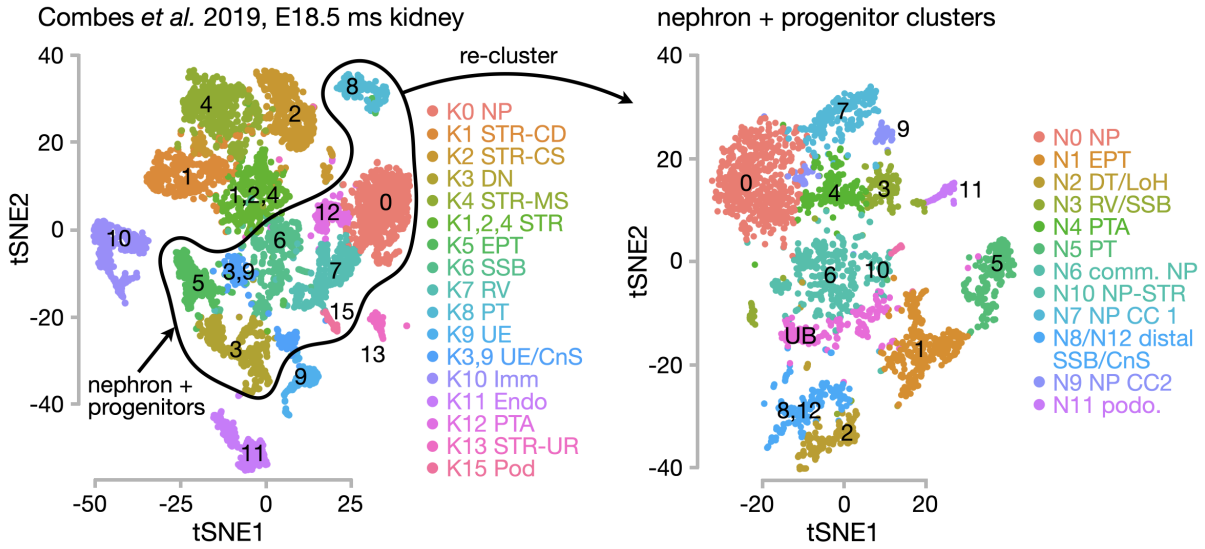

Fig. S7: Re-clustering of Combes *et al.* 2019 whole E18.5 mouse kidney scRNA-seq data. tSNE plots annotated by cell type. *Left*, The nephron lineage clusters outlined in black from the whole kidney data were re-clustered, *right*, for use in Fig. 3. These clusters closely resemble those in Figs. 1A and 4A in Combes *et al.* 2019.

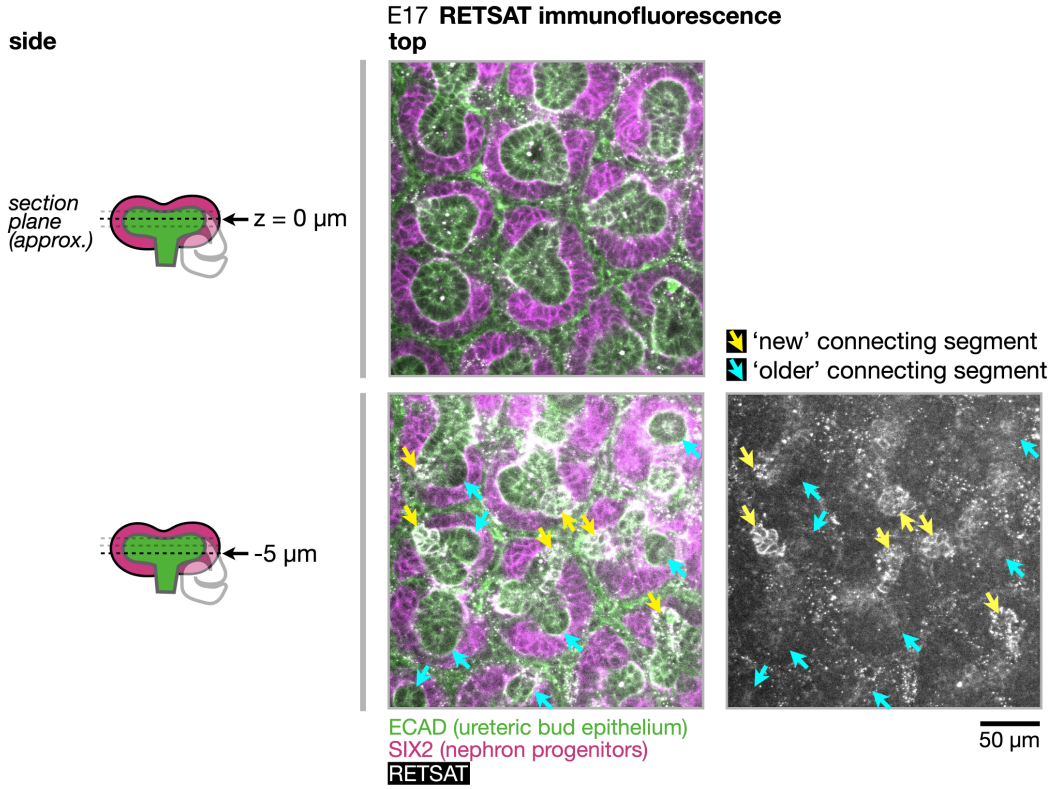

Fig. S8: Confocal immunofluorescence validation of RETSAT expression. Whole-mount confocal immunofluorescence images in E17 mouse embryonic kidney at ~niche mid-plane and at -5 µm in *z* showing RETSAT protein-level expression in 'new' connecting segments (yellow arrows).

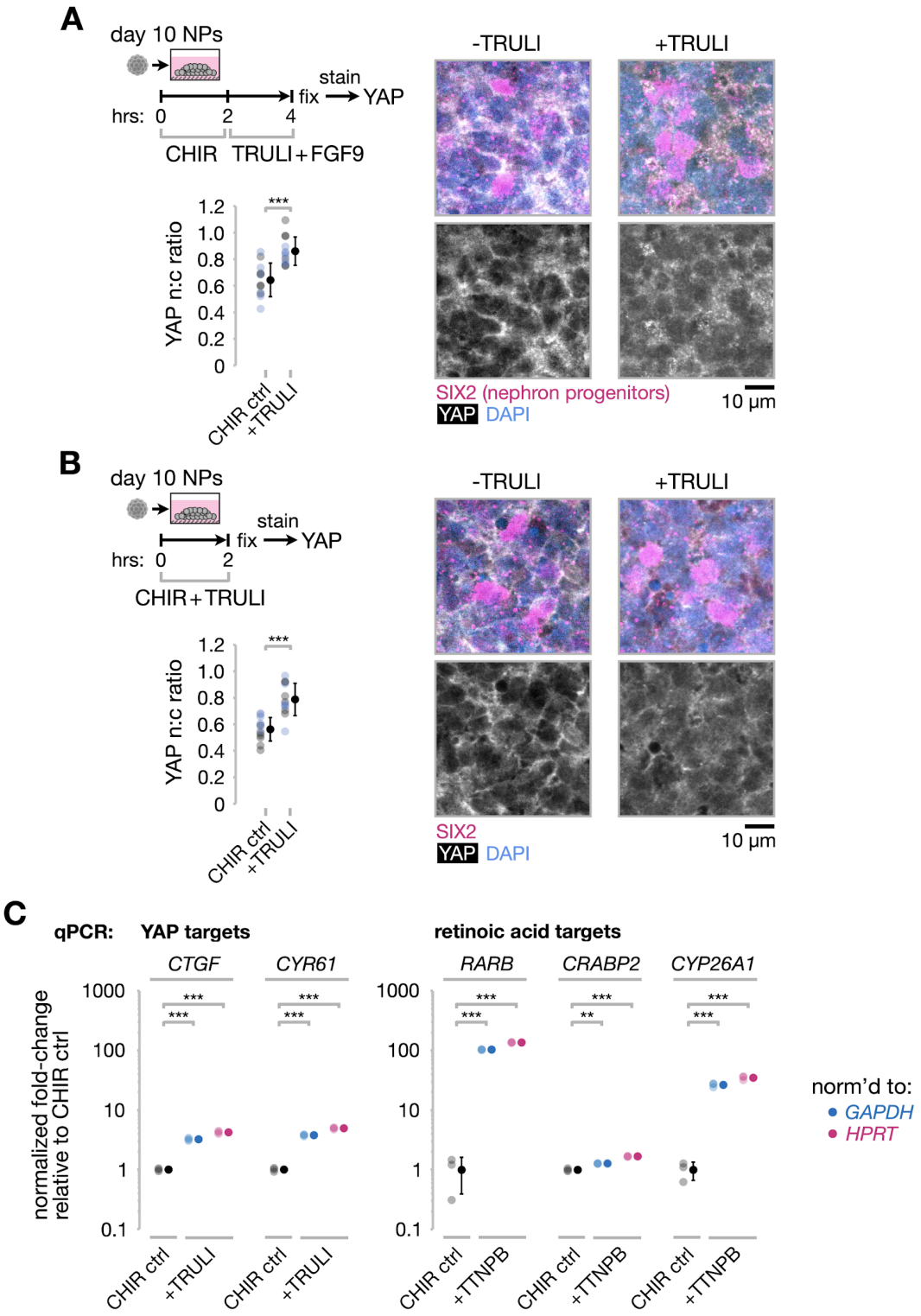

Fig. S9: Validation of TRULI and TTNPB activity in human iPSC-derived nephron progenitor 'puck' organoids. (**A**) *Left*, Plot of YAP nuclear-to-cytoplasmic (n:c) ratio (a metric for YAP activation) in day 10 nephron progenitor (NP) organoids fixed after staggered 7 µM CHIR and 4 µM TRULI treatments relative to CHIR-only controls (n = 6 cells from each of two replicate pairs of organoids per comparison indicated by black and blue marker colors, mean ± S.D., unpaired t-test ***p < 0.001). *Right*, representative immunofluorescence micrographs at approximate organoid mid-planes. (**B**) Similar data for overlapping 7 µM CHIR and 4 µM TRULI treatments relative to CHIR-only controls. (**C**) qPCR quantitation of YAP and retinoic acid transcriptional target expression in nephron progenitor organoids treated as in (B) for overlapping 7 µM CHIR and 4 µM TRULI or 0.1 µM TTNPB treatments relative to CHIR-only controls (n = 3 reactions per condition, 8 organoids pooled per reaction, mean ± S.D., unpaired t-test **p < 0.01, ***p < 0.001). Expression was normalized to either *GAPDH* or *HPRT* housekeeping transcripts.

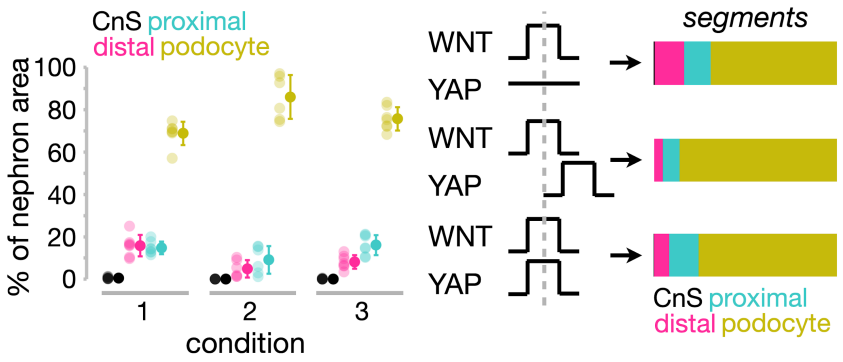

Fig. S10: TRULI experiment organoid composition. Plot and schematic of nephron composition by cell type for conditions 1-3 in Fig. 5 at day 25, $n > 5$ pucks per condition, mean ± S.D.

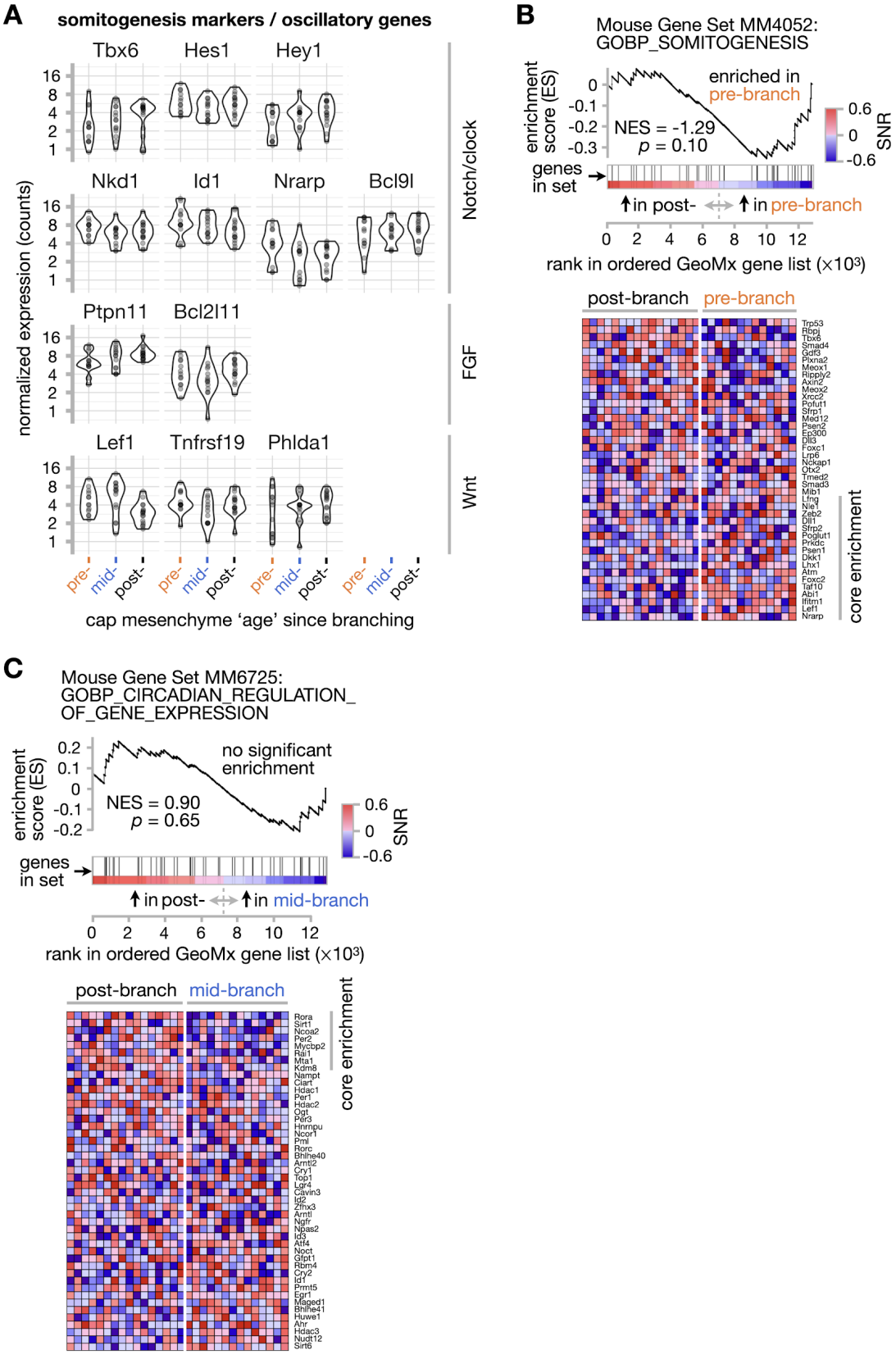

Fig. S11: GeoMx gene expression and gene-set enrichment analysis for somitogenesis and circadian clocks in nephron progenitors over branching life-cycle. (**A**) Expression of oscillatory genes associated with somitogenesis (From Dequeant et al., 2006, *Science*) in cap mesenchyme GeoMx data. (**B**) Gene-set enrichment analysis (GSEA) for somitogenesis genes in pre- vs. post-branching nephron progenitor niches showing enrichment score plot, 'ticker-tape' plot showing gene rankings in GeoMx transcriptome, and expression heat-map ordered by gene rank. NES, normalized enrichment score. (**C**) Similar GSEA analysis for circadian regulation of gene expression gene set in mid- vs. post-branching nephron progenitor niches.

Supplementary Tables

Table S1: Curated marker and signaling gene lists relevant to nephron progenitor renewal/differentiation.

Curated marker gene list	Notes
Cited1	Lawlor 2019 Fig. 5. Guo 2021: regulator/marker of self-renewing NPCs. Karner 2011 Wnt9b target gene. Reginensi 2013: Yap-dependent gene.
Mest	Lawlor 2019 Fig. 5. Kanwar 2022: Treatment of metanephroi, harvested at day 13 of gestation with MEST-specific antisense oligodeoxynucleotide resulted in a dose-dependent decrease in the size of the explants and the nephron population
Crym	Lawlor 2019 Fig. 5. Combes 2019 fig. 1,5 NP cluster 0
Meis2	Lawlor 2019 Fig. 5. Clugston 2022: "Our analysis suggests that Meis2 and Hmga2 are potential targets of the let-7 family of miRNAs in nephron progenitors (Fig. 2), with decreased expression of Meis2 and Hmga2 associated with increasing expression of the let-7 family members in differentiating or aging nephron progenitors. The transcription factor Meis2 is strongly expressed in nephron progenitors and the renal stroma during kidney development, and is linked to the regulation of cell proliferation in other contexts."
Gas1	Lawlor 2019 Fig. 5. Kann 2015 WT1 targets Gas1 to maintain nephron progenitor cells by modulating FGF signals. Gas1 -> FGFs -> Akt -> NP proliferation. Park 2012 Class II gene cobound by Six2 and b-catenin in NPs. Class II genes are expressed in the CM and repressed by canonical Wnt signaling upon differentiation in response to BIO relative to DMSO-treated controls.
Ttc28	Lawlor 2019 Fig. 5. AKA TPRBK. Izumiyama 2012: "...essential for the formation and integrity of the midbody, hence we postulated that TPRBK plays a critical role in the progress of mitosis and cytokinesis during mammalian cell cycle."
Six2	Lawlor 2019 Fig. 5. Guo 2021: regulator/marker of self-renewing NPCs
Hmcn1	Lawlor 2019 Fig. 5. Kopan 2014.
Tril	Lawlor 2019 Fig. 5. Kim 2021(3): "In Xenopus embryos, Tril triggers degradation of the transforming growth factor β (Tgf-ß) family inhibitor, Smad7. This enhances bone morphogenetic protein (Bmp) signaling to enable ventral mesoderm to commit to a blood fate. Here, we show that Tril simultaneously dampens Nodal signaling by catalytically activating the ubiquitin ligase NEDD4 Like (Nedd4l). Nedd4l then targets Nodal receptors for degradation."
Robo2	Lawlor 2019 Fig. 5. Miao 2021: Gdnf-Ret pathway, expressed in NPs.
Eya1	Lawlor 2019 Fig. 5. Guo 2021: regulator/marker of self-renewing NPCs. Miao 2021: genetically upstream of Gdnf, positive regulator for its activation. Kopan 2014: regulates Six2.
Meox1	Lawlor 2019 Fig. 5. Kopan 2014.
Ptpn13	Lawlor 2019 Fig. 5. Saras 1997: AKA PTPL1, PTP-BAS, hPTP1E, or FAP-1. "...a complex between PTPL1 and PARG1 may function as a powerful negative regulator of Rho signaling, acting both on Rho itself and on tyrosine phosphorylated components in the Rho signal transduction pathway." Wang 2022(5): "Mechanistically, PTPL1 knockdown induced the activation of the Proto-oncogene tyrosine-protein kinase SRC (Src)/Extracellular regulated MAP kinase (ERK) pathway and thereby promoted yes-associated protein (YAP1) nuclear translocation and activation." Similar negative regulation of YAP by Ptpn14 in Liu 2013.
Emx2	Lawlor 2019 Fig. 5. Guo 2021: associates with NPC differentiation in vivo. Lindstrom 2018: PTA/RV I.
Arl4c	Lawlor 2019 Fig. 5. Matsumoto 2016: Wnt/betacat target.
Lhx1	Lawlor 2019 Fig. 5. Guo 2021: associated with induction of nephrogenesis
Wnt4	Karner 2011 Wnt9b target gene. Lawlor 2019 Fig. 5. Lindstrom 2015 Fig. 4. distal & beta cat target. Guo 2021: Associated with induction of nephrogenesis
Bmp4	Brown 2013. redundant with BMP7. Guo 2021: Early induced NPCs. Kim 2019(4): BMP7 functions predominantly as a heterodimer with BMP2 or BMP4 during mammalian embryogenesis.
Bmp2	Georgas 2009: Distal RV/connecting segment. "Bmp2 expression has previously been implicated in the regulation of ureteric epithelial proliferation (Hartwig et al., 2005). Distal Bmp2 signaling may regulate UT branching and mitosis, again to facilitate fusion between the RV and the UT. Using a BMP signaling reporter mouse, it has been shown that SMAD signaling in the kidney is present in the ureteric compartment, but not the tips (Blank et al., 2008). Upon closer inspection signaling is biased to the side of the UT adjacent to the Bmp2-expressing RV connecting segment." Kim 2019(4): BMP7 functions predominantly as a heterodimer with BMP2 or BMP4 during mammalian embryogenesis.
Gpc3	Hartwig 2005: Glypican 3, modulates BMP2/SMAD1/4 signaling. Expressed in UB and CM.
Lef1	Lindstrom 2015 Fig. 4. Target genes of β-catenin (Lef1 and Ccnd1)
Ltbp1	Georgas 2009 Fig 1. Latent TGF-beta binding protein.
Wt1	Guo 2021: NPC specification/maintenance. Pritchard-Jones 1990, Stark 1994.
Ccnd1	Cyclin D1. Lindstrom 2015: target genes of β-catenin (Lef1 and Ccnd1). Cruz 2020: Hh/Smo/Gli target. Should be MAPK target as well.
Pax2	Lindstrom 2018: Primed NPC I. Cruz 2020: Hh/Smo/Gli target. Reginensi 2013: Yap-dependent gene. Guo 2021: NPC specification/maintenance. Georgas 2009: "Pax8 is a transcription factor which acts cooperatively with Pax2 to regulate cell survival and lineage specification of the early metanephric mesenchyme and later, the differentiation of distal nephron segments (Bouchard et al., 2002; Narlis et al., 2007)."
Cdh4	Karner 2011 Wnt9b target gene. Georgas 2009: R-cadherin, PTA/RV
Notch2	Combes 2019 NP cluster 3. Georgas 2009: "Notch2 and its ligand Jag1, are critical for proximal tubule and glomerular development (Cheng et al., 2007; McCright et al., 2001; McCright et al., 2002). Disruption of Notch2 results in a loss of Cadherin-6 expression in the kidney (Cheng et al., 2007), hence undoubtedly disrupting RV patterning."
Pdgfra	Combes 2019 NP cluster 7. Lawlor 2019: nephron progenitor cells (two clusters, Six2, Cited1, with cluster separation based on a weak stromal signature e.g. Pdgfra)
Fgf8	Guo 2021: associated with induction of nephrogenesis. Early induced NPCs.
Axin2	Lindstrom 2015 Fig. 4. beta cat target
Hoxa11	Guo 2021: NPC specification/maintenance
Hoxd11	Guo 2021: NPC specification/maintenance
Sall1	Guo 2021: NPC specification/maintenance. Cruz 2020: Hh/Smo/Gli target.
Osr1	Guo 2021: regulator/marker of self-renewing NPCs
Cxcr4	Karner 2011 Wnt9b target gene. Guo 2021: associates with NPC differentiation in vivo
Hnf1b	Ng 2023: committed epithelium. Involved in completion of MET. "...reported to antagonise Wnt/b-Catenin signalling by both directly repressing LEF1 gene expression and by competitively binding and antagonising TCF/LEF1-target genes."
Gdnf	Miao 2021: nephron progenitor marker. Genetically downstream of Eya1. Karner 2011 Wnt9b target gene.
Uncx	Karner 2011 Wnt9b target gene. Miao 2021: nephron progenitor marker.
Sox11	Miao 2021 Fig. 3.
Sox4	O'Brien 2018(2): "... genes expressed in nephron progenitors and implicated in progenitor maintenance and self-renewal including Six2, Pax2, Sall1, Sox4, and Gas1"
Hey1	Lindstrom 2018: primed NPC I/II. Notch pathway early target gene. Guo 2021: Early induced NPCs.
Hes1	Lindstrom 2018. Chen and Al-Awqati, 2005.
Igfbp5	Lindstrom 2018 (human)
Lypd1	Lindstrom 2018 (human)
Pax8	Karner 2011 Wnt9b target gene. Lawlor 2019 Fig. 5. Georgas 2009: "Pax8 is a transcription factor which acts cooperatively with Pax2 to regulate cell survival and lineage specification of the early metanephric mesenchyme and later, the differentiation of distal nephron segments (Bouchard et al., 2002; Narlis et al., 2007)."

Curated signaling gene list	Notes
Unc5c	Combes 2019 receptor-ligand interactions with cortical stroma, Miao 2021 Fig. 5.
Fzd2	Combes 2019 receptor-ligand interactions with cortical stroma, Miao 2021 Fig. 5.
Itga8	Karner 2011 Wnt9b target gene. Combes 2019 receptor-ligand interactions with cortical stroma, UB, Miao 2021 Fig. 5.
Fgfr1	Combes 2019 receptor-ligand interactions with cortical stroma, UB, Miao 2021 Fig. 5. Trueb 2013.
Fgf1	Combes 2019 receptor-ligand interactions with cortical stroma, UB, Miao 2021 Fig. 5. Trueb 2013. Brown 2011: Maintains/supports proliferation (?) of Cited1+ (naïve) NPCs.
Pdgfc	Combes 2019 receptor-ligand interactions with cortical stroma, Miao 2021 Fig. 5.
Ntf3	Combes 2019 receptor-ligand interactions with cortical stroma.
Tnc	Tenascin C. Combes 2019 receptor-ligand interactions with cortical stroma, Miao 2021 Fig. 5. Menon 2018: stromal. Interesting potential role in integrin, fak/ERK/MAPK signaling and proliferation. Muller 1997: tenascin C is ligand for integrin a8b1 but knockout is silent; argues expression increases too late to explain phenotype in a8b1 deficient animals.
Bmp7	Brown 2013. Combes 2019: influences organization of the cortical stroma (Oxburgh 2004), shown in cap mesenchyme. Kann 2015: Bmp7 is a WT1 target gene (Hartwig et al., 2010) that promotes NPC proliferation by activation of JNK MAPK. Combes 2019 receptor-ligand interactions with cortical stroma, UB, Miao 2021 Fig. 5. Kim 2019(4): BMP7 functions predominantly as a heterodimer with BMP2 or BMP4 during mammalian embryogenesis.
Rspo1	Combes 2019 receptor-ligand interactions with UB. Vidal 2020: RSPO1 and RSPO3 act in a functionally redundant manner to permit WNT/b- catenin signalling and their genetic deletion leads to a rapid decline of nephron progenitors
Rspo3	Combes 2019 receptor-ligand interactions with UB, Miao 2021 Fig. 5. Vidal 2020: "RSPO1 and RSPO3 act in a functionally redundant manner to permit WNT/b-catenin signalling and their genetic deletion leads to a rapid decline of nephron progenitors"
Fzd7	Combes 2019 receptor-ligand interactions with UB. O'Brien 2018.
Cdh2	Combes 2019 receptor-ligand interactions with UB, Miao 2021 Fig. 5.
Gfra1	Combes 2019 receptor-ligand interactions with UB.
Acvr2b	Activin A receptor. Combes 2019 receptor-ligand interactions with UB.
Fgf9	Miao 2021 Fig. 5. Karner 2011 Wnt9b target gene.
Fgf10	Reginensi 2013: Yap-dependent gene.
Col2a1	Combes 2019 Fig. 2. Menon 2018, "COL2A1 is expressed in the developing mouse kidney (Wada et al., 1997) but its cell specificity and functional role remain to be elucidated." Detected in seq data, same in Vanslambrouk 2022. Potential stromal marker.
Bmpr1a	Combes 2019 Fig. 2, Miao 2021 Fig. 5.
Tgfbi	Combes 2019 Fig. 2. Schwab 2003: expressed in cap mesenchyme but not present after at latest S-shaped body stage, induced by TGFB1 and prevents cell adhesion, secreted, RGD-containing collagen-associated protein, and is thought to interact with the ECM. Brunskill 2011.
Smo	Miao 2021 Fig. 5. Rowan 2018 (in stroma).
Gli1	Rowan 2018: "...expression of Gli1, a downstream HH signaling target, in the kidney cortex, including the developing kidney capsule and the nephrogenic zone."
Gli3	Miao 2021 Fig. 5.
Mycn	N-myc. Cruz 2020: Hh/Smo/Gli target. Pan 2017(2): c- and N-myc cooperate with β-catenin to activate the Wnt9b/β- catenin progenitor renewal program in vivo
Myc	C-myc. PI3K/Akt target. Pan & Carroll 2017: "...c- and N-myc cooperate with β-catenin to activate the Wnt9b/β- catenin progenitor renewal program in vivo"
Foxc1	Miao 2021 Fig. 5. Motojima 2022: "Foxc1 and Foxc2 are indispensable for the maintenance of nephron and stromal progenitors in the developing kidney"
Slit2	Miao 2021 Fig. 5. Grieshammer: Slit2-Robo2 signaling involved in restricting supernumerary UBs.
Fgfr2	Miao 2021 Fig. 5. Walker 2016.
Tcf7	Guo 2021: activating TCF/LEF factor mediating txn'l response elicited by Wnt/b-catenin.
Tcf7l1	Guo 2021: repressive TCF/LEF factor mediating txn'l response elicited by Wnt/b-catenin
Tcf7l2	Guo 2021: repressive TCF/LEF factor mediating txn'l response elicited by Wnt/b-catenin
Tgfbr2	Rowan 2018, downstream of Hh-Gli signaling. crucial for nephron progenitor diff. vs. prolif & accumulation
Meox2	Reginensi 2013: Yap-dependent gene.
Traf1	Reginensi 2013: Yap-dependent gene. TNF receptor-associated factor 1. Gerhardt 2021: prosurvival in ischemia-reperfusion injury model.
Capn6	Reginensi 2013: Yap-dependent gene. Calpain-6, a microtubule-stabilizing protein, regulates Rac1 activity and cell motility through interaction with GEF-H1.
Id1	Dumbrava 2021: TGFB target gene. Lindstrom 2018: Primed NPC.
Smad7	Dumbrava 2021: TGFB target gene, antagonizes TGFB signaling.

Table S2: Primer sequences used for organoid qPCR analysis.

gene	forward primer	reverse primer
CRABP2	CCTAGGAGTCTACGGGGACC	ATCACATTCACCCCCAGCAC
CTGF	CGCACAAGGGCCTATTCTGT	GAGCACCATCTTTGGCGGT
CYP26A1	GCTGCGATCAAGCTCTGGG	GAACTTCCTCCGCTGCAGTA
CYR61	GATTCGATGCCTCCGAGGTG	TCCATTCCAAAAACAGGGAGC
GAPDH	AGGTCGGAGTCAACGGATTT	TGGAATTTGCCATGGGTGGA
HPRT	TGCTTTCCTTGGTCAGGCAG	TTCAAATCCAACAAAGTCTGGC
RARβ	ATCGGCACACTGCTCAATCAAT	GGTTTGTACACTCGAGGGGG

Supplementary Files

The following supplementary files are available at https://doi.org/10.6084/m9.figshare.24585114.v1

1) GeoMx slice image and FIJI ROIs.
2) GeoMx sequencing data (.dcc, .pkc, and sample annotation files).
3) HCR RNA-smFISH probe sequences.
4) Curated gene lists.

References

1. Short, K.M., Combes, A.N., Lefevre, J., Ju, A.L., Georgas, K.M., Lamberton, T., Cairncross, O., Rumballe, B.A., McMahon, A.P., Hamilton, N.A., et al. (2014). Global quantification of tissue dynamics in the developing mouse kidney. Dev. Cell *29*, 188–202.

2. Hoy, W.E., Hughson, M.D., Bertram, J.F., Douglas-Denton, R., and Amann, K. (2005). Nephron number, hypertension, renal disease, and renal failure. J. Am. Soc. Nephrol. *16*, 2557–2564.

3. Bueters, R.R., van de Kar, N.C., and Schreuder, M.F. (2013). Adult renal size is not a suitable marker for nephron numbers: an individual patient data meta-analysis. Kidney Blood Press. Res. *37*, 540–546.

4. Perl, A.J., Schuh, M.P., and Kopan, R. (2022). Regulation of nephron progenitor cell lifespan and nephron endowment. Nat. Rev. Nephrol. *18*, 683–695.

5. Yermalovich, A.V., Osborne, J.K., Sousa, P., Han, A., Kinney, M.A., Chen, M.J., Robinton, D.A., Montie, H., Pearson, D.S., Wilson, S.B., et al. (2019). Lin28 and let-7 regulate the timing of cessation of murine nephrogenesis. Nat. Commun. *10*, 168.

6. Keller, G., Zimmer, G., Mall, G., Ritz, E., and Amann, K. (2003). Nephron number in patients with primary hypertension. N. Engl. J. Med. *348*, 101–108.

7. Howden, S.E., Vanslambrouck, J.M., Wilson, S.B., Tan, K.S., and Little, M.H. (2019). Reporter-based fate mapping in human kidney organoids confirms nephron lineage relationships and reveals synchronous nephron formation. EMBO Rep. *20*. 10.15252/embr.201847483.

8. Little, M.H. (2021). Returning to kidney development to deliver synthetic kidneys. Dev. Biol. *474*, 22–36.

9. Smyth, I.M. (2021). Development of the metanephric kidney. Curr. Top. Dev. Biol. *143*, 111–150.

10. Brown, A.C., Adams, D., de Caestecker, M., Yang, X., Friesel, R., and Oxburgh, L. (2011). FGF/EGF signaling regulates the renewal of early nephron progenitors during embryonic development. Development *138*, 5099–5112.

11. Barak, H., Huh, S.-H., Chen, S., Jeanpierre, C., Martinovic, J., Parisot, M., Bole-Feysot, C., Nitschké, P., Salomon, R., Antignac, C., et al. (2012). FGF9 and FGF20 maintain the stemness of nephron progenitors in mice and man. Dev. Cell *22*, 1191–1207.

12. Ihermann-Hella, A., Hirashima, T., Kupari, J., Kurtzeborn, K., Li, H., Kwon, H.N., Cebrian, C., Soofi, A., Dapkunas, A., Miinalainen, I., et al. (2018). Dynamic MAPK/ERK Activity Sustains Nephron Progenitors through Niche Regulation and Primes Precursors for Differentiation. Stem Cell Reports *11*, 912–928.

13. Kurtzeborn, K., Kwon, H.N., Iaroshenko, V., Faisal, I., Ambrož, M., Jin, X., Qureshi, T., Kupari, J., Ihermann-Hella, A., Väänänen, J., et al. (2022). Comparative whole-genome transcriptome analysis in renal cell populations reveals high tissue specificity of MAPK/ERK targets in embryonic kidney. BMC Biol. *20*, 112.

14. Lindström, N.O., Carragher, N.O., and Hohenstein, P. (2015). The PI3K pathway balances self-renewal and differentiation of nephron progenitor cells through β-catenin signaling. Stem Cell Reports *4*, 551–560.

15. Carroll, T.J., Park, J.-S., Hayashi, S., Majumdar, A., and McMahon, A.P. (2005). Wnt9b plays a central role in the regulation of mesenchymal to epithelial transitions underlying organogenesis of the mammalian urogenital system. Dev. Cell *9*, 283–292.

16. Park, J.-S., Valerius, M.T., and McMahon, A.P. (2007). Wnt/beta-catenin signaling regulates nephron induction during mouse kidney development. Development *134*, 2533–2539.

17. Park, J.-S., Ma, W., O'Brien, L.L., Chung, E., Guo, J.-J., Cheng, J.-G., Valerius, M.T., McMahon, J.A., Wong, W.H., and McMahon, A.P. (2012). Six2 and Wnt regulate self-renewal and commitment of nephron progenitors through shared gene regulatory networks. Dev. Cell *23*, 637–651.

18. Karner, C.M., Das, A., Ma, Z., Self, M., Chen, C., Lum, L., Oliver, G., and Carroll, T.J. (2011). Canonical Wnt9b signaling balances progenitor cell expansion and differentiation during kidney development. Development *138*, 1247–1257.

19. Reginensi, A., Scott, R.P., Gregorieff, A., Bagherie-Lachidan, M., Chung, C., Lim, D.-S., Pawson, T., Wrana, J., and McNeill, H. (2013). Yap- and Cdc42-dependent nephrogenesis and morphogenesis during mouse kidney development. PLoS Genet. *9*, e1003380.

20. Das, A., Tanigawa, S., Karner, C.M., Xin, M., Lum, L., Chen, C., Olson, E.N., Perantoni, A.O., and Carroll, T.J. (2013). Stromal-epithelial crosstalk regulates kidney progenitor cell differentiation. Nat. Cell Biol. *15*, 1035–1044.

21. Wang, H., Yang, Y., Sharma, N., Tarasova, N.I., Timofeeva, O.A., Winkler-Pickett, R.T., Tanigawa, S., and Perantoni, A.O. (2010). STAT1 activation regulates proliferation and differentiation of renal progenitors. Cell. Signal. *22*, 1717–1726.

22. Tanigawa, S., Sharma, N., Hall, M.D., Nishinakamura, R., and Perantoni, A.O. (2015). Preferential Propagation of Competent SIX2+ Nephronic Progenitors by LIF/ROCKi Treatment of the Metanephric Mesenchyme. Stem Cell Reports *5*, 435–447.

23. Brown, A.C., Muthukrishnan, S.D., Guay, J.A., Adams, D.C., Schafer, D.A., Fetting, J.L., and Oxburgh, L. (2013). Role for compartmentalization in nephron progenitor differentiation. Proc. Natl. Acad. Sci. U. S. A. *110*, 4640–4645.

24. Blank, U., Brown, A., Adams, D.C., Karolak, M.J., and Oxburgh, L. (2009). BMP7 promotes proliferation of nephron progenitor cells via a JNK-dependent mechanism. Development *136*, 3557–3566.

25. Lindström, N.O., Lawrence, M.L., Burn, S.F., Johansson, J.A., Bakker, E.R.M., Ridgway, R.A., Chang, C.-H., Karolak, M.J., Oxburgh, L., Headon, D.J., et al. (2015). Integrated β-catenin, BMP, PTEN, and Notch signalling patterns the nephron. Elife *3*, e04000.

26. Boyle, S.C., Kim, M., Valerius, M.T., McMahon, A.P., and Kopan, R. (2011). Notch pathway activation can replace the requirement for Wnt4 and Wnt9b in mesenchymal-to-epithelial transition of nephron stem cells. Development *138*, 4245–4254.

27. Chung, E., Deacon, P., Marable, S., Shin, J., and Park, J.-S. (2016). Notch signaling promotes nephrogenesis by downregulating Six2. Development *143*, 3907–3913.

28. Lindström, N.O., De Sena Brandine, G., Tran, T., Ransick, A., Suh, G., Guo, J., Kim, A.D., Parvez, R.K., Ruffins, S.W., Rutledge, E.A., et al. (2018). Progressive Recruitment of Mesenchymal Progenitors Reveals a Time-Dependent Process of Cell Fate Acquisition in Mouse and Human Nephrogenesis. Dev. Cell *45*, 651–660.e4.

29. Viola, J.M., Liu, J., Prahl, L.S., Huang, A., Chan, T.J., Hayward-Lara, G., Porter, C.M., Shi, C., Zhang, J., and Hughes, A.J. (2023). Tubule jamming in the developing mouse kidney creates cyclical mechanical stresses in nephron-forming niches. bioRxiv, 2022.06.03.494718. 10.1101/2022.06.03.494718.

30. Ramalingam, H., Fessler, A.R., Das, A., Valerius, M.T., Basta, J., Robbins, L., Brown, A.C., Oxburgh, L., McMahon, A.P., Rauchman, M., et al. (2018). Disparate levels of beta-catenin activity determine nephron progenitor cell fate. Dev. Biol. *440*, 13–21.

31. Mugford, J.W., Yu, J., Kobayashi, A., and McMahon, A.P. (2009). High-resolution gene expression

analysis of the developing mouse kidney defines novel cellular compartments within the nephron progenitor population. Dev. Biol. *333*, 312–323.

32. Lawlor, K.T., Zappia, L., Lefevre, J., Park, J.-S., Hamilton, N.A., Oshlack, A., Little, M.H., and Combes, A.N. (2019). Nephron progenitor commitment is a stochastic process influenced by cell migration. Elife *8*. 10.7554/eLife.41156.

33. Combes, A.N., Lefevre, J.G., Wilson, S., Hamilton, N.A., and Little, M.H. (2016). Cap mesenchyme cell swarming during kidney development is influenced by attraction, repulsion, and adhesion to the ureteric tip. Dev. Biol. *418*, 297–306.

34. Guo, Q., Kim, A., Li, B., Ransick, A., Bugacov, H., Chen, X., Lindström, N., Brown, A., Oxburgh, L., Ren, B., et al. (2021). A β-catenin-driven switch in TCF/LEF transcription factor binding to DNA target sites promotes commitment of mammalian nephron progenitor cells. Elife *10*. 10.7554/eLife.64444.

35. Mederacke, M., Conrad, L., Doumpas, N., Vetter, R., and Iber, D. (2023). Geometric effects position renal vesicles during kidney development. Cell Rep. *42*, 113526.

36. O'Brien, L.L., Combes, A.N., Short, K.M., Lindström, N.O., Whitney, P.H., Cullen-McEwen, L.A., Ju, A., Abdelhalim, A., Michos, O., Bertram, J.F., et al. (2018). Wnt11 directs nephron progenitor polarity and motile behavior ultimately determining nephron endowment. Elife *7*. 10.7554/eLife.40392.

37. Oxburgh, L., Chu, G.C., Michael, S.K., and Robertson, E.J. (2004). TGFbeta superfamily signals are required for morphogenesis of the kidney mesenchyme progenitor population. Development *131*, 4593–4605.

38. Viola, J.M., Liu, J., Huang, A., Grindel, S.H., Prahl, L.S., and Hughes, A.J. (2023). Rho/ROCK activity tunes cell compartment segregation and differentiation in nephron-forming niches. bioRxiv, 2023.11.08.566308. 10.1101/2023.11.08.566308.

39. Merritt, C.R., Ong, G.T., Church, S.E., Barker, K., Danaher, P., Geiss, G., Hoang, M., Jung, J., Liang, Y., McKay-Fleisch, J., et al. (2020). Multiplex digital spatial profiling of proteins and RNA in fixed tissue. Nat. Biotechnol. *38*, 586–599.

40. Choi, H.M.T., Chang, J.Y., Trinh, L.A., Padilla, J.E., Fraser, S.E., and Pierce, N.A. (2010). Programmable in situ amplification for multiplexed imaging of mRNA expression. Nat. Biotechnol. *28*, 1208–1212.

41. Dirks, R.M., and Pierce, N.A. (2004). Triggered amplification by hybridization chain reaction. Proc. Natl. Acad. Sci. U. S. A. *101*, 15275–15278.

42. Choi, H.M.T., Schwarzkopf, M., Fornace, M.E., Acharya, A., Artavanis, G., Stegmaier, J., Cunha, A., and Pierce, N.A. (2018). Third-generation in situ hybridization chain reaction: multiplexed, quantitative, sensitive, versatile, robust. Development *145*. 10.1242/dev.165753.

43. Abdulla, M., Traiki, T.B., Vaali-Mohammed, M.-A., El-Wetidy, M.S., Alhassan, N., Al-Khayal, K., Zubaidi, A., Al-Obeed, O., and Ahmad, R. (2022). Targeting MUCL1 protein inhibits cell proliferation and EMT by deregulating β-catenin and increases irinotecan sensitivity in colorectal cancer. Int. J. Oncol. *60*. 10.3892/ijo.2022.5312.

44. Renz, P.F., Spies, D., Tsikrika, P., Wutz, A., Beyer, T.A., and Ciaudo, C. (2020). Inhibition of FGF and TGF-β Pathways in hESCs Identify STOX2 as a Novel SMAD2/4 Cofactor. Biology *9*. 10.3390/biology9120470.

45. Zhou, W., Ouyang, J., Li, J., Liu, F., An, T., Cheng, L., Kuo, Z.C., Zhang, C., and He, Y. (2021). MRPS17 promotes invasion and metastasis through PI3K/AKT signal pathway and could be potential prognostic marker for gastric cancer. J. Cancer *12*, 4849.

46. Subramanian, A., Tamayo, P., Mootha, V.K., Mukherjee, S., Ebert, B.L., Gillette, M.A., Paulovich, A., Pomeroy, S.L., Golub, T.R., Lander, E.S., et al. (2005). Gene set enrichment analysis: a knowledge-based approach for interpreting genome-wide expression profiles. Proc. Natl. Acad. Sci. U. S. A. *102*, 15545–15550.

47. Combes, A.N., Phipson, B., Lawlor, K.T., Dorison, A., Patrick, R., Zappia, L., Harvey, R.P., Oshlack, A., and Little, M.H. (2019). Single cell analysis of the developing mouse kidney provides deeper insight into marker gene expression and ligand-receptor crosstalk. Development *146*, dev178673.

48. Miao, Z., Balzer, M.S., Ma, Z., Liu, H., Wu, J., Shrestha, R., Aranyi, T., Kwan, A., Kondo, A., Pontoglio, M., et al. (2021). Single cell regulatory landscape of the mouse kidney highlights cellular differentiation programs and disease targets. Nat. Commun. *12*, 2277.

49. Vidal, V.P., Jian-Motamedi, F., Rekima, S., Gregoire, E.P., Szenker-Ravi, E., Leushacke, M., Reversade, B., Chaboissier, M.-C., and Schedl, A. (2020). R-spondin signalling is essential for the maintenance and differentiation of mouse nephron progenitors. Elife *9*. 10.7554/eLife.53895.

50. Menon, R., Otto, E.A., Kokoruda, A., Zhou, J., Zhang, Z., Yoon, E., Chen, Y.-C., Troyanskaya, O., Spence, J.R., Kretzler, M., et al. (2018). Single-cell analysis of progenitor cell dynamics and lineage specification in the human fetal kidney. Development *145*. 10.1242/dev.164038.

51. Schwab, K., Patterson, L.T., Aronow, B.J., Luckas, R., Liang, H.-C., and Potter, S.S. (2003). A catalogue of gene expression in the developing kidney. Kidney Int. *64*, 1588–1604.

52. Rowan, C.J., Li, W., Martirosyan, H., Erwood, S., Hu, D., Kim, Y.-K., Sheybani-Deloui, S., Mulder, J., Blake, J., Chen, L., et al. (2018). Hedgehog-GLI signaling in Foxd1-positive stromal cells promotes murine nephrogenesis via TGFβ signaling. Development *145*. 10.1242/dev.159947.

53. Pan, X., Karner, C.M., and Carroll, T.J. (2017). Myc cooperates with β-catenin to drive gene expression in nephron progenitor cells. Development *144*, 4173–4182.

54. Walker, K.A., Sims-Lucas, S., and Bates, C.M. (2016). Fibroblast growth factor receptor signaling in kidney and lower urinary tract development. Pediatr. Nephrol. *31*, 885–895.

55. Dumbrava, M.G., Lacanlale, J.L., Rowan, C.J., and Rosenblum, N.D. (2021). Transforming growth factor beta signaling functions during mammalian kidney development. Pediatr. Nephrol. *36*, 1663–1672.

56. Clugston, A., Bodnar, A., Cerqueira, D.M., Phua, Y.L., Lawler, A., Boggs, K., Pfenning, A.R., Ho, J., and Kostka, D. (2022). Chromatin accessibility and microRNA expression in nephron progenitor cells during kidney development. Genomics *114*, 278–291.

57. Kopan, R., Chen, S., and Little, M. (2014). Nephron progenitor cells: shifting the balance of self-renewal and differentiation. Curr. Top. Dev. Biol. *107*, 293–331.

58. Georgas, K., Rumballe, B., Valerius, M.T., Chiu, H.S., Thiagarajan, R.D., Lesieur, E., Aronow, B.J., Brunskill, E.W., Combes, A.N., Tang, D., et al. (2009). Analysis of early nephron patterning reveals a role for distal RV proliferation in fusion to the ureteric tip via a cap mesenchyme-derived connecting segment. Dev. Biol. *332*, 273–286.

59. O'Brien, L.L., Guo, Q., Bahrami-Samani, E., Park, J.-S., Hasso, S.M., Lee, Y.-J., Fang, A., Kim, A.D., Guo, J., Hong, T.M., et al. (2018). Transcriptional regulatory control of mammalian nephron progenitors revealed by multi-factor cistromic analysis and genetic studies. PLoS Genet. *14*, e1007181.

60. D'Cruz, R., Stronks, K., Rowan, C.J., and Rosenblum, N.D. (2020). Lineage-specific roles of hedgehog-GLI signaling during mammalian kidney development. Pediatr. Nephrol. *35*, 725–731.

61. Narlis, M., Grote, D., Gaitan, Y., Boualia, S.K., and Bouchard, M. (2007). Pax2 and pax8 regulate branching morphogenesis and nephron differentiation in the developing kidney. J. Am. Soc. Nephrol. *18*, 1121–1129.

62. Fetting, J.L., Guay, J.A., Karolak, M.J., Iozzo, R.V., Adams, D.C., Maridas, D.E., Brown, A.C., and Oxburgh, L. (2014). FOXD1 promotes nephron progenitor differentiation by repressing decorin in the embryonic kidney. Development *141*, 17–27.

63. Izumiyama, T., Minoshima, S., Yoshida, T., and Shimizu, N. (2012). A novel big protein TPRBK possessing 25 units of TPR motif is essential for the progress of mitosis and cytokinesis. Gene *511*, 202–217.

64. Lindström, N.O., Tran, T., Guo, J., Rutledge, E., Parvez, R.K., Thornton, M.E., Grubbs, B., McMahon, J.A., and McMahon, A.P. (2018). Conserved and Divergent Molecular and Anatomic Features of Human and Mouse Nephron Patterning. J. Am. Soc. Nephrol. *29*, 825–840.

65. Kann, M., Bae, E., Lenz, M.O., Li, L., Trannguyen, B., Schumacher, V.A., Taglienti, M.E., Bordeianou, L., Hartwig, S., Rinschen, M.M., et al. (2015). WT1 targets Gas1 to maintain nephron progenitor cells by modulating FGF signals. Development *142*, 1254–1266.

66. Bais, A.S., Cerqueira, D.M., Clugston, A., Bodnar, A.J., Ho, J., and Kostka, D. (2021). Single-cell RNA sequencing reveals differential cell cycle activity in key cell populations during nephrogenesis. Sci. Rep. *11*, 22434.

67. Trueb, B., Amann, R., and Gerber, S.D. (2013). Role of FGFRL1 and other FGF signaling proteins in early kidney development. Cell. Mol. Life Sci. *70*, 2505–2518.

68. Brunskill, E.W., Lai, H.L., Jamison, D.C., Potter, S.S., and Patterson, L.T. (2011). Microarrays and RNA-Seq identify molecular mechanisms driving the end of nephron production. BMC Dev. Biol. *11*, 15.

69. Shah, S., Hecht, A., Pestell, R., and Byers, S.W. (2003). Trans-repression of β-Catenin Activity by Nuclear Receptors*. J. Biol. Chem. *278*, 48137–48145.

70. Yasuhara, R., Yuasa, T., Williams, J.A., Byers, S.W., Shah, S., Pacifici, M., Iwamoto, M., and Enomoto-Iwamoto, M. (2010). Wnt/β-catenin and retinoic acid receptor signaling pathways interact to regulate chondrocyte function and matrix turnover. J. Biol. Chem. *285*, 317–327.

71. Dequéant, M.-L., Glynn, E., Gaudenz, K., Wahl, M., Chen, J., Mushegian, A., and Pourquié, O. (2006). A complex oscillating network of signaling genes underlies the mouse segmentation clock. Science *314*, 1595–1598.

72. Stark, K., Vainio, S., Vassileva, G., and McMahon, A.P. (1994). Epithelial transformation of metanephric mesenchyme in the developing kidney regulated by Wnt-4. Nature *372*, 679–683.

73. Magella, B., Adam, M., Potter, A.S., Venkatasubramanian, M., Chetal, K., Hay, S.B., Salomonis, N., and Potter, S.S. (2018). Cross-platform single cell analysis of kidney development shows stromal cells express Gdnf. Dev. Biol. *434*, 36–47.

74. Hilliard, S., Tortelote, G., Liu, H., Chen, C.-H., and El-Dahr, S.S. (2022). Single-Cell Chromatin and Gene-Regulatory Dynamics of Mouse Nephron Progenitors. J. Am. Soc. Nephrol. *33*, 1308–1322.

75. Lindström, N.O., Guo, J., Kim, A.D., Tran, T., Guo, Q., De Sena Brandine, G., Ransick, A., Parvez, R.K., Thornton, M.E., Baskin, L., et al. (2018). Conserved and Divergent Features of Mesenchymal Progenitor Cell Types within the Cortical Nephrogenic Niche of the Human and Mouse Kidney. J. Am. Soc. Nephrol. *29*, 806–824.

76. Bruno, S., and Darzynkiewicz, Z. (1992). Cell cycle dependent expression and stability of the nuclear protein detected by Ki-67 antibody in HL-60 cells. Cell Prolif. *25*, 31–40.

77. Morizane, R., Lam, A.Q., Freedman, B.S., Kishi, S., Valerius, M.T., and Bonventre, J.V. (2015). Nephron organoids derived from human pluripotent stem cells model kidney development and injury. Nat. Biotechnol. *33*, 1193–1200.

78. Gupta, A.K., Ivancic, D.Z., Naved, B.A., Wertheim, J.A., and Oxburgh, L. (2021). An efficient method to generate kidney organoids at the air-liquid interface. J Biol Methods *8*, e150.

79. Lawlor, K.T., Vanslambrouck, J.M., Higgins, J.W., Chambon, A., Bishard, K., Arndt, D., Er, P.X., Wilson, S.B., Howden, S.E., Tan, K.S., et al. (2021). Cellular extrusion bioprinting improves kidney organoid reproducibility and conformation. Nat. Mater. *20*, 260–271.

80. Takasato, M., Er, P.X., Chiu, H.S., Maier, B., Baillie, G.J., Ferguson, C., Parton, R.G., Wolvetang, E.J., Roost, M.S., Chuva de Sousa Lopes, S.M., et al. (2015). Kidney organoids from human iPS cells contain multiple lineages and model human nephrogenesis. Nature *526*, 564–568.

81. Combes, A.N., Zappia, L., Er, P.X., Oshlack, A., and Little, M.H. (2019). Single-cell analysis reveals congruence between kidney organoids and human fetal kidney. Genome Med. *11*, 3.

82. Wu, H., Uchimura, K., Donnelly, E.L., Kirita, Y., Morris, S.A., and Humphreys, B.D. (2018). Comparative Analysis and Refinement of Human PSC-Derived Kidney Organoid Differentiation with Single-Cell Transcriptomics. Cell Stem Cell *23*, 869–881.e8.

83. McNeill, H., and Reginensi, A. (2017). Lats1/2 Regulate Yap/Taz to Control Nephron Progenitor Epithelialization and Inhibit Myofibroblast Formation. J. Am. Soc. Nephrol. *28*, 852–861.

84. Huang, B., Zeng, Z., Li, H., Li, Z., Chen, X., Guo, J., Zhang, C.C., Schreiber, M.E., Vonk, A.C., Xiang, T., et al. (2023). Modeling kidney development, disease, and plasticity with clonal expandable nephron progenitor cells and nephron organoids. bioRxiv. 10.1101/2023.05.25.542343.

85. Bagherie-Lachidan, M., Reginensi, A., Pan, Q., Zaveri, H.P., Scott, D.A., Blencowe, B.J., Helmbacher, F., and McNeill, H. (2015). Stromal Fat4 acts non-autonomously with Dchs1/2 to restrict the nephron progenitor pool. Development *142*, 2564–2573.

86. Mao, Y., Francis-West, P., and Irvine, K.D. (2015). Fat4/Dchs1 signaling between stromal and cap mesenchyme cells influences nephrogenesis and ureteric bud branching. Development *142*, 2574–2585.

87. Kastan, N., Gnedeva, K., Alisch, T., Petelski, A.A., Huggins, D.J., Chiaravalli, J., Aharanov, A., Shakked, A., Tzahor, E., Nagiel, A., et al. (2021). Small-molecule inhibition of Lats kinases may promote Yap-dependent proliferation in postmitotic mammalian tissues. Nat. Commun. *12*, 3100.

88. Bugacov, H., Der, B., Kim, S., Lindström, N.O., and McMahon, A.P. (2023). Canonical Wnt transcriptional complexes are essential for induction of nephrogenesis but not maintenance or proliferation of nephron progenitors. bioRxiv. 10.1101/2023.08.20.554044.

89. Takayama, M., Miyatake, K., and Nishida, E. (2014). Identification and characterization of retinoic acid-responsive genes in mouse kidney development. Genes Cells *19*, 637–649.

90. Marlier, A., and Gilbert, T. (2004). Expression of retinoic acid-synthesizing and -metabolizing enzymes during nephrogenesis in the rat. Gene Expr. Patterns *5*, 179–185.

91. Wingert, R.A., Selleck, R., Yu, J., Song, H.-D., Chen, Z., Song, A., Zhou, Y., Thisse, B., Thisse, C., McMahon, A.P., et al. (2007). The cdx genes and retinoic acid control the positioning and segmentation of the zebrafish pronephros. PLoS Genet. *3*, 1922–1938.

92. Deacon, P., Concodora, C.W., Chung, E., and Park, J.-S. (2019). β-catenin regulates the formation of multiple nephron segments in the mouse kidney. Sci. Rep. *9*, 15915.

93. Araoka, T., Mae, S.-I., Kurose, Y., Uesugi, M., Ohta, A., Yamanaka, S., and Osafune, K. (2014). Efficient and rapid induction of human iPSCs/ESCs into nephrogenic intermediate mesoderm using small molecule-based differentiation methods. PLoS One *9*, e84881.

94. Beard, R.L., Chandraratna, R.A., Colon, D.F., Gillett, S.J., Henry, E., Marler, D.K., Song, T., Denys, L., Garst, M.E., and Arefieg, T. (1995). Synthesis and structure-activity relationships of stilbene retinoid analogs substituted with heteroaromatic carboxylic acids. J. Med. Chem. *38*, 2820–2829.

95. Hubaud, A., and Pourquié, O. (2014). Signalling dynamics in vertebrate segmentation. Nat. Rev. Mol. Cell Biol. *15*, 709–721.

96. Hubaud, A., Regev, I., Mahadevan, L., and Pourquié, O. (2017). Excitable Dynamics and Yap-Dependent Mechanical Cues Drive the Segmentation Clock. Cell *171*, 668–682.e11.

97. Dan, H., Ruan, T., and Sampogna, R.V. (2020). Circadian Clock Regulation of Developmental Time in the Kidney. Cell Rep. *31*, 107661.

98. Batourina, E., Gim, S., Bello, N., Shy, M., Clagett-Dame, M., Srinivas, S., Costantini, F., and Mendelsohn, C. (2001). Vitamin A controls epithelial/mesenchymal interactions through Ret expression. Nat. Genet. *27*, 74–78.

99. Diez del Corral, R., Olivera-Martinez, I., Goriely, A., Gale, E., Maden, M., and Storey, K. (2003). Opposing FGF and retinoid pathways control ventral neural pattern, neuronal differentiation, and segmentation during body axis extension. Neuron *40*, 65–79.

100. Muller, U., Wang, D., Denda, S., Meneses, J.J., Pedersen, R.A., and Reichardt, L.F. Integrin ab1 Is Critically Important for Epithelial–Mesenchymal Interactions during Kidney Morphogenesis. Cell.

101. Ohmori, T., Tanigawa, S., Kaku, Y., Fujimura, S., and Nishinakamura, R. (2015). Sall1 in renal stromal progenitors non-cell autonomously restricts the excessive expansion of nephron progenitors. Sci. Rep. *5*, 15676.

102. Wanek, N., Muneoka, K., Holler-Dinsmore, G., Burton, R., and Bryant, S.V. (1989). A staging system for mouse limb development. J. Exp. Zool. *249*, 41–49.

103. Barak, H., and Boyle, S.C. (2011). Organ culture and immunostaining of mouse embryonic kidneys. Cold Spring Harb. Protoc. *2011*, db.prot5558.

104. Zollinger, D.R., Lingle, S.E., Sorg, K., Beechem, J.M., and Merritt, C.R. (2020). GeoMx™ RNA Assay: High Multiplex, Digital, Spatial Analysis of RNA in FFPE Tissue. Methods Mol. Biol. *2148*, 331–345.

105. Reeves, J., Divakar, P., Ortogero, N., Griswold, M., Yang, Z., Zimmerman, S., Vitancol, R., and Henderson, D. Analyzing GeoMx-NGS RNA Expression Data with GeomxTools. https://bioconductor.org/packages/devel/workflows/vignettes/GeoMxWorkflows/inst/doc/GeomxTools_RNA-NGS_Analysis.html.

106. Seurat - guided clustering tutorial https://satijalab.org/seurat/articles/pbmc3k_tutorial.html.

107. Prahl, L.S., Viola, J.M., Liu, J., and Hughes, A.J. (2023). The developing murine kidney actively negotiates geometric packing conflicts to avoid defects. Dev. Cell *58*, 110–120.e5.

108. Combes, A.N., Short, K.M., Lefevre, J., Hamilton, N.A., Little, M.H., and Smyth, I.M. (2014). An integrated pipeline for the multidimensional analysis of branching morphogenesis. Nat. Protoc. *9*, 2859–2879.

109. Berg, S., Kutra, D., Kroeger, T., Straehle, C.N., Kausler, B.X., Haubold, C., Schiegg, M., Ales, J., Beier, T., Rudy, M., et al. (2019). ilastik: interactive machine learning for (bio)image analysis. Nat. Methods *16*, 1226–1232.

110. Morabito, A., Malkmus, J., Pancho, A., Zuniga, A., Zeller, R., and Sheth, R. (2023). Optimized protocol for whole-mount RNA fluorescent in situ hybridization using oxidation-mediated autofluorescence reduction on mouse embryos. STAR Protoc *4*, 102603.

111. Zimmerman, S.G., Peters, N.C., Altaras, A.E., and Berg, C.A. (2013). Optimized RNA ISH, RNA FISH and protein-RNA double labeling (IF/FISH) in Drosophila ovaries. Nat. Protoc. *8*, 2158–2179.

112. Ibarra-García-Padilla, R., Howard, A.G.A., 4th, Singleton, E.W., and Uribe, R.A. (2021). A protocol for whole-mount immuno-coupled hybridization chain reaction (WICHCR) in zebrafish embryos and larvae. STAR Protoc *2*, 100709.

113. Wang, W.X., Douglas, T.R., Zhang, H., Bhattacharya, A., Rothenbroker, M., Jia, Z., Muffat, J., Li, Y., and Chou, L.Y.T. (2022). origamiFISH allows universal, label-free, single molecule visualization of DNA origami nanodevices across biological samples. bioRxiv. 10.1101/2022.09.19.508533.

114. Vanslambrouck, J.M., Wilson, S.B., Tan, K.S., Soo, J.Y.-C., Scurr, M., Spijker, H.S., Starks, L.T., Neilson, A., Cui, X., Jain, S., et al. (2019). A Toolbox to Characterize Human Induced Pluripotent Stem Cell-Derived Kidney Cell Types and Organoids. J. Am. Soc. Nephrol. *30*, 1811–1823.

115. Morizane, R., and Bonventre, J.V. (2017). Generation of nephron progenitor cells and kidney organoids from human pluripotent stem cells. Nat. Protoc. *12*, 195–207.

116. Satija, R., Farrell, J.A., Gennert, D., Schier, A.F., and Regev, A. (2015). Spatial reconstruction of single-cell gene expression data. Nat. Biotechnol. *33*, 495–502.

117. Butler, A., Hoffman, P., Smibert, P., Papalexi, E., and Satija, R. (2018). Integrating single-cell transcriptomic data across different conditions, technologies, and species. Nat. Biotechnol. *36*, 411–420.

118. GSEA User Guide https://www.gsea-msigdb.org/gsea/doc/GSEAUserGuideFrame.html.

119. Weber, P., Flores, R.E., Kiefer, M.F., and Schupp, M. (2020). Retinol Saturase: More than the Name Suggests. Trends Pharmacol. Sci. *41*, 418–427.

120. Moise, A.R., Kuksa, V., Imanishi, Y., and Palczewski, K. (2004). Identification of all-trans-retinol:all-trans-13,14-dihydroretinol saturase. J. Biol. Chem. *279*, 50230–50242.

121. Rosselot, C., Spraggon, L., Chia, I., Batourina, E., Riccio, P., Lu, B., Niederreither, K., Dolle, P., Duester, G., Chambon, P., et al. (2010). Non-cell-autonomous retinoid signaling is crucial for renal development. Development *137*, 283–292.

122. Colpitts, T.L., Billing, P., Granados, E., Hayden, M., Hodges, S., Roberts, L., Russell, J., Friedman, P., and Stroupe, S. (2002). Identification and immunohistochemical characterization of a mucin-like glycoprotein expressed in early stage breast carcinoma. Tumour Biol. *23*, 263–278.

123. Conley, S.J., Bosco, E.E., Tice, D.A., Hollingsworth, R.E., Herbst, R., and Xiao, Z. (2016). HER2 drives Mucin-like 1 to control proliferation in breast cancer cells. Oncogene *35*, 4225–4234.

124. Kufe, D.W. (2013). MUC1-C oncoprotein as a target in breast cancer: activation of signaling pathways and therapeutic approaches. Oncogene *32*, 1073–1081.

125. van Hijfte, L., Geurts, M., Vallentgoed, W.R., Eilers, P.H.C., Sillevis Smitt, P.A.E., Debets, R., and French, P.J. (2023). Alternative normalization and analysis pipeline to address systematic bias in NanoString GeoMx Digital Spatial Profiling data. iScience *26*, 105760.

126. Xu, J., Liu, H., Park, J.-S., Lan, Y., and Jiang, R. (2014). Osr1 acts downstream of and interacts synergistically with Six2 to maintain nephron progenitor cells during kidney organogenesis. Development *141*, 1442–1452.

127. McCarthy, S.S., Karolak, M., and Oxburgh, L. (2022). Smad4 controls proliferation of interstitial cells in the neonatal kidney. Development *149*. 10.1242/dev.199984.

128. Johnson, S.A., Zitserman, D., and Roegiers, F. (2016). Numb regulates the balance between Notch recycling and late-endosome targeting in Drosophila neural progenitor cells. Mol. Biol. Cell *27*, 2857–2866.

129. Hansson, M.L., Behmer, S., Ceder, R., Mohammadi, S., Preta, G., Grafström, R.C., Fadeel, B., and Wallberg, A.E. (2012). MAML1 acts cooperatively with EGR1 to activate EGR1-regulated promoters: implications for nephrogenesis and the development of renal cancer. PLoS One *7*, e46001.

130. Li, B., Zhu, C., Dong, L., Qin, J., Xiang, W., Davidson, A.J., Feng, S., Wang, Y., Shen, X., Weng, C., et al. (2020). ADAM10 mediates ectopic proximal tubule development and renal fibrosis through Notch signalling. J. Pathol. *252*, 274–289.

131. Schmidt-Ott, K.M., Masckauchan, T.N.H., Chen, X., Hirsh, B.J., Sarkar, A., Yang, J., Paragas, N., Wallace, V.A., Dufort, D., Pavlidis, P., et al. (2007). beta-catenin/TCF/Lef controls a differentiation-associated transcriptional program in renal epithelial progenitors. Development *134*, 3177–3190.

132. Billings, S.E., Pierzchalski, K., Butler Tjaden, N.E., Pang, X.-Y., Trainor, P.A., Kane, M.A., and Moise, A.R. (2013). The retinaldehyde reductase DHRS3 is essential for preventing the formation of excess retinoic acid during embryonic development. FASEB J. *27*, 4877–4889.

133. Mendelsohn, C., Ruberte, E., LeMeur, M., Morriss-Kay, G., and Chambon, P. (1991). Developmental analysis of the retinoic acid-inducible RAR-beta 2 promoter in transgenic animals. Development *113*, 723–734.

134. Bohnenpoll, T., Weiss, A.-C., Labuhn, M., Lüdtke, T.H., Trowe, M.-O., and Kispert, A. (2017). Retinoic acid signaling maintains epithelial and mesenchymal progenitors in the developing mouse ureter. Sci. Rep. *7*, 14803.

135. Balmer, J.E., and Blomhoff, R. (2002). Gene expression regulation by retinoic acid. J. Lipid Res. *43*, 1773–1808.

136. Chal, J., and Pourquié, O. (2017). Making muscle: skeletal myogenesis in vivo and in vitro. Development *144*, 2104–2122.

137. Goldbeter, A., Gonze, D., and Pourquié, O. (2007). Sharp developmental thresholds defined through bistability by antagonistic gradients of retinoic acid and FGF signaling. Dev. Dyn. *236*, 1495–1508.

138. Cunningham, T.J., Zhao, X., Sandell, L.L., Evans, S.M., Trainor, P.A., and Duester, G. (2013). Antagonism between retinoic acid and fibroblast growth factor signaling during limb development. Cell Rep. *3*, 1503–1511.

139. Diez del Corral, R., and Storey, K.G. (2004). Opposing FGF and retinoid pathways: a signalling switch that controls differentiation and patterning onset in the extending vertebrate body axis. Bioessays *26*, 857–869.

140. Malpel, S., Mendelsohn, C., and Cardoso, W.V. (2000). Regulation of retinoic acid signaling during lung morphogenesis. Development *127*, 3057–3067.

141. Ng-Blichfeldt, J.-P., Schrik, A., Kortekaas, R.K., Noordhoek, J.A., Heijink, I.H., Hiemstra, P.S., Stolk, J., Königshoff, M., and Gosens, R. (2018). Retinoic acid signaling balances adult distal lung epithelial progenitor cell growth and differentiation. EBioMedicine *36*, 461–474.

142. Tonami, K., Kurihara, Y., Aburatani, H., Uchijima, Y., Asano, T., and Kurihara, H. (2007). Calpain 6 is involved in microtubule stabilization and cytoskeletal organization. Mol. Cell. Biol. *27*, 2548–2561.